FEASIBILITY ASSESSMENT AND RESEARCH RESULTS REPORT

Prepared For

California Independent System Operator (CA ISO)

Prepared By

Consortium for Electric Reliability Technology Solutions (CERTS)

Funded By

California Public Interest Energy Research
Transmission Research Program

Date: Revised June 20, 2008

CERTS
CONSORTIUM FOR ELECTRIC RELIABILITY TECHNOLOGY SOLUTIONS

The work described in this report was coordinated by the Consortium for Electric Reliability Technology Solutions with funding provided by the California Energy Commission, Public Interest Energy Research Program, through the University of California/California Institute of Energy Efficiency under Contract No. 500-02-004, MR-041.

PREPARED FOR:

California Independent System Operator

PREPARED BY:

Electric Power Group

Manu Parashar, Ph.D. - Principal Investigator

Wei Zhou - Investigator

Montana Tech

Dan Trudnowski, Ph.D. - Consultant

Pacific Northwest National Laboratory

Yuri Makarov, Ph.D. - Principal Consultant

University of Wisconsin, Madison

Ian Dobson, Ph.D. - Consultant

DATE: Revised June 20, 2008

Acknowledgements

Special thanks to California ISO staff Mr. Jim Hiebert, Mr. Brian O'Hearn, Mr. Brian Murry, Mr. Paul Bleuss, Mr. Greg Tillitson, Mr. Eric Whitley and Mr. Nan Liu for their consultations to the project and support for the RTDMS system.

Mr. Dave Hawkins (California ISO) for his expertise, comprehensive support, and advices.

Dr. Yuri V. Makarov (PNNL) and Prof. Ian Dobson, (University of Wisconsin-Madison) for their role in suggesting methodologies on applying phasor technology to stability nomogram, literature review, participation in the brainstorm meetings, expertise and essential advices.

Prof. Dan Trudnowski (Montana Tech), for providing the algorithms for monitoring oscillatory modes under ambient system conditions and his support in the prototype development.

Mr William Mittelstadt, Mr Ken Martin (BPA), Dr John Hauer, Dr Henry Huang, Dr Ning Zhou (PNNL), Prof. John Pierre (University of Wyoming) for sharing their expertise and advise on the mode meter algorithm evaluation.

Mr. Jim Cole (California Institute for Energy Efficiency) for initiating and support of this project, and participants of the TAC meeting for their thoughtful suggestions.

Mr. Joseph Eto (Lawrence Berkeley National Lab) for his support.

Parashar, Manu, Wei Zhou, Dan Trudnowski, Yuri Marakov, Ian Dobson. Consortium for Electric Reliability Technology Solutions (CERTS). 2008. Phasor Technology Applications Feasibility Assessment and Research Results Report. California Energy Commission, PIER Transmission Research Program. CEC-500-2008-XXX**.**

Preface

The Public Interest Energy Research (PIER) Program supports public interest energy research and development that will help improve the quality of life in California by bringing environmentally safe, affordable, and reliable energy services and products to the marketplace.

The PIER Program, managed by the California Energy Commission (Energy Commission), conducts public interest research, development, and demonstration (RD&D) projects to benefit California.

The PIER Program strives to conduct the most promising public interest energy research by part nering with RD&D entities, including individuals, businesses, utilities, and public or private res earch institutions.

PIER funding efforts are focused on the following RD&D program areas:

- Buildings End-Use Energy Efficiency
- Energy Innovations Small Grants
- Energy-Related Environmental Research
- Energy Systems Integration
- Environmentally Preferred Advanced Generation
- Industrial/Agricultural/Water End-Use Energy Efficiency
- Renewable Energy Technologies
- Transportation

Real Time System Operations (RTSO) 2006 - 2007 is the final report for the Real Time System Operations project (contract number 500-03-024 MR041 conducted by the Consortium for Electric Reliability Technology Solutions (CERTS). The information from this project contributes to PIER's Transmission Research Program.

For more information about the PIER Program, please visit the Energy Commission's website at www.energy.ca.gov/pier or contact the Energy Commission at 916-654-5164.

Table of Contents

LIST OF FIGURES

1.0 INTRODUCTION

Phasor technology is one of the key technologies on the horizon that holds great promise towards improving grid reliability, relieving transmission congestion, and addressing some of today's operational challenges within the electric industry. This technology complements existing SCADA systems by providing the high sub-second resolution and global visibility to address the new emerging need for wide area grid monitoring, while continuing to use existing SCADA infrastructure for local monitoring and control.

Recent advances in the field of phasor technologies offer new possibilities in providing the industry with tools and applications to address the blackout recommendations and to tackle reliability management and operational challenges faced by system operators and reliability coordinators. The utilization of real-time phasor measurements in the fields of visualization, monitoring, protection, and control is expected to revolutionize the way in which the power grid of the future can identify and manage reliability threats and will respond to contingencies.

Phasor measurement data provide precise real-time direct monitoring capability of the power system dynamics (beyond the static view currently available via SCADA) at a very high rate. They also have the capability of accurately estimating and dynamically tracking various system parameters that provide a quantitative assessment of the health of system under the current operating condition and the prevalent contingency. In particular, synchronized phasor measurements provide an accurate sequence of snap-shots of the power system behavior at a very high rate (30 samples per second) along with precise timing information. The timing information is essential for real-time continuous estimation of system parameters that classify the power system. A precise estimate of the load, generator and/or network parameters consequently provide the most accurate assessment of the system limits of the current operating system. This time series data along with real-time system parameter estimates based on the data can be utilized to improve stability nomogram monitoring, small signal stability monitoring, voltage stability monitoring and system frequency response assessment. A main advantage of such methodologies is that they can measure actual system states and performance and do not rely on offline studies for its assessment, nor do they rely on comprehensive system models, which can be outdated or/and inaccurate.

1.1. Objective

A California PIER funded multi-year project plan aimed at developing Real-Time Applications of Phasors for Monitoring, Alarming and Control is currently in place. One of the tasks within this plan is to research and evaluate the feasibility of using phasors for (1) improving stability nomograms as a first step towards wide area control, (2) monitoring small-signal stability, (3) measuring key sensitivities related to voltage stability or dynamic stability, (4) assessing interconnection frequency response. (4) and applying graph theory concepts for pattern recognition.

The objective of the feasibility assessment study was to propose several approaches for using these time synchronized, high resolution PMU (Phasor Measurement Unit) measurements and

possibly other EMS/SCADA data for better assessment of the system operating conditions with respect to their stability limits. Some initial results and research prototypes that were developed as under this project are also discussed. These prototypes have been developed on the Real Time Dynamics Monitoring System (RTDMS™) which is the CERTS platform conducting phasor research.

1.2. Nomogram Validation

The existing nomograms are built in the course of off-line power flow, voltage, transient and post-transient stability simulations for a "worst case" scenario. The "worst case scenario" may include

- The most limiting contingency conditions,
- Combinations of the critical (most influential) parameters,
- Most influential fault locations (for transient stability studies),
- Critical load demand conditions, and
- Generation dispatches.

The necessity of providing robustness to the nomograms is implied by the "worst case" approach. Thus the nomograms are designed to define secure operating conditions for all real-life operating situations, even if these situations deviate from the conditions simulated by the operations engineers when they develop the nomograms.

One more reason that makes the existing nomograms even more *conservative* is the necessity to select two or three most influential (critical) parameters to describe the nomograms in a way that addresses a variety of real-life situations resulting from errors accumulated by system parameters that are not included in the nomogram.

The nomograms are usually represented graphically on a plane of two critical parameters using piecewise linear approximation of the nomograms' boundaries. The boundaries usually have a composite nature describing different types of operating limits such as thermal constraints, voltage and transient stability limits, and "cascading constraints". If the third critical parameter is involved, the nomogram is represented as a family of limiting curves represented by the so-called "diagonal axis". Each of the curves along the "diagonal axis" corresponds to a certain value of the third critical parameters.

The pre-calculated nomograms are used in the scheduling process, operations planning, and real-time dispatch. With the implementation of the new California ISO market design, these nomograms will be incorporated as additional constraints limiting the Security Constrained Unit Commitment (SCUC) and Security Constrained Economic Dispatch (SCED) procedures.

™ Built upon GRID-3P Platform, U.S. Patent 7,233,843. Electric Power Group. All rights reserved.

Therefore, the limits specified by the nomograms contribute to the costs associated with congestion and will influence the forward and real-time market prices in California.

The need for a more dynamically adjustable nomogram is well understood at the California ISO, and several ideas have been generated around the potential use of manually or automatically adjusted nomograms. This approach could potentially decrease the existing congestion cost in California which are estimated at up to $500 million a year. The idea of using the PMU data to improve and adjust the existing nomograms was also proposed by the California ISO.

In general terms, the proposed concept deals with the tradeoff between the pre-calculated fixed operating limits that are based on extensive computations (which tend to be more conservative due to the uncertainty about the applications) and the limits calculated in real time and adjusted to the current system conditions (which must be computationally less expensive, but based on better knowledge of current conditions). By shifting the focus from some of the pre-calculated operating constraints to real-time calculations, it is possible to build more flexible nomograms.

Specifically, the use of real-time measurements provided by PMUs and the results of real-time stability assessment applications can complement the existing nomograms by making the pre-calculated nomograms less conservative. These measurements can also provide data to select critical nomogram parameters for visualization based on real-time information and determine new areas and situations where additional nomograms may be required.

At the same time, there are several limiting factors that need to be considered while addressing these tasks:

- The nomograms reflect various contingency and system conditions. The real-time measurements reflect just the current system state/contingency, and therefore are not indicative of potential stability problems that might happen for the same load and generation pattern under different contingency conditions or under heavier loading conditions
- Although PMUs can track the dynamics of certain grid variables in real time, there are only a limited in number of PMUs distributed over a wide area. Since PMUs do not provide full observability of the system state – additional data from the state estimation and SCADA may be required
- The number and location of the existing PMUs may not be adequate to the task of monitoring of local stability limits such as those induced by voltage stability problems

Nevertheless, phasor measurements do provide wide area observability of system swing or oscillatory dynamics where the state estimator performance is too slow, and certain approaches that exploit these attributes can be suggested for nomogram validation purposes.

1.3. Small-Signal Stability Monitoring

Low frequency electrical modes exist in the system that are of interest because they characterize the stability of the power system and limit the power flow across regions. While there is a danger that such modes can lead to instability in the power system following a sizable contingency in the system, there is also the risk of these modes becoming unstable (i.e., negatively damped) due to gradual changes in the system. The ability to continuously track the damping associated with these low frequency modes in real time and under normal conditions would therefore be a valuable tool for operators and power system engineers.

Recently there have been efforts to identify these low frequency modes under normal operating conditions. The concept is that there is broadband ambient noise present in the power system mainly due to random load variations in the system. The random variations act as a constant low-level excitation to the electromechanical dynamics in the power system and are observed in the power-flows through, or phase angle differences across, a transmission line. Assuming that the variations are truly random over the frequency range of interest (the oscillations typically lie between 0.1 to 2Hz), the spectral content of power-flows across tie-lines obtained from phasor measurements can be used to estimate the inter-area modal frequencies and damping. Operators would be alarmed if the damping of these modes falls below predetermined thresholds (e.g. 3% or 5%).

1.4. Voltage Stability and Measurement Based Sensitivity Computations

Sensitivity information, such as voltage sensitivities at critical buses to increased loading, have traditionally been computed by power system analysis tools that require complete modeling information. With the precise time synchronization and the diversity in the measurement sets from PMUs (i.e. voltage and current phasors, frequency, MW/MVAR flows), it is possible to correlate changes in one of these monitored metrics to another in real-time and, therefore, directly measure and quantify such dependencies.

While voltages at key buses and their respective voltage sensitivities to additional loading are important indicators of voltage stability, for a complete voltage security assessment it is also essential to monitor and track the loading margins to the point-of-collapse and also account for contingencies. Fortunately, phasor measurements at a load bus or from a key interface also contain enough information to estimate the voltage stability margin and define a Voltage Stability Index for it. It is a well-known fact that for a simplistic two-bus system with a constant power load (i.e., a constant source behind an impedance and a load), the maximum loadability condition occurs when the voltage drop across the source impedance is equal to the voltage across the load. Hence, the idea is to use the phasor measurements at the bus to dynamically track in real-time the two-bus equivalent of the system (a.k.a. Thevenin equivalent). As these Thevenin parameters are being tracked dynamically, they reflect any changes that may occur in the power system operating conditions and consequently provide the most accurate assessment of loadability estimates.

1.5. Frequency Response Assessment

Recent task force studies show evidence of degrading reliability performance over the years. For example, the Frequency Response Characteristic (FRC), which is a measure of the Interconnection's primary frequency control to significant change in load-generation balance and the initial defense towards arresting its decline and supporting the system frequency, is at a decline. FRC survey results gathered for the observed frequency deviations over various outages indicate that the Eastern Interconnection's Frequency Response has declined from about -3,750 MW/0.1Hz in 1994 to less than -3,200 MW/0.1Hz in 2002 (i.e., an 18% decline) while load and generation grew nearly 20% over the same period [13]. A similar decline has also been observed in the Western Interconnection's Frequency Response. Theoretically, Frequency Response should have increased proportionally with generation and load. In the past many control areas carried full reserves for their individual largest contingency and some for multiple contingencies. However, competitive pressures and greater reliance on reserve sharing groups (RSG) have reduced reserves and safety margins. If these trends continue, they may jeopardize the interconnection's ability to withstand large disturbances and move the system closer to automatic under frequency load shedding.

The sub-second resolution associated phasor measurements is sufficient to accurately track the frequency response following a major disturbance such as a generation trip. By monitoring the frequency trends during the first 2-10 seconds after such an event, (i.e. time scales typically associated with the primary control), and mapping this change in frequency to associated MW change in the system (which may also be available directly from PMU measurements), one can build a database of the interconnection Frequency Response over time.

1.6. Graph Theory based Pattern Recognition

Graph theory techniques can be used to characterize, monitor and assess the global behavior of the power grid, as well as to detect anomalies in the system. In particular, correlation between measured phase angle signals may be used to develop network graph whose noted denote the correlation in phasor measurements. One could then apply graph-theoretic tools to segment the measurements into a small subset of signals for real time monitoring by a human operator. The network-level analysis approach may be further applied to perform anomaly detection at the topological level, where the entire network might be undergoing significant but incremental changes in response to an anomalous event as well as to identify the focal root cause of the anomalous behavior by evaluating graph-theoretic distance measures.

2.0 METHODOLOGIES FOR USING PHASORS FOR STABILITY NOMOGRAMS

2.1. Improving Existing Nomograms using Real-Time Phasor Measurements

The real-time operating conditions can deviate from the simulated conditions that have been used to build the pre-calculated existing nomograms. The existing nomograms have been developed using a very limited number of critical parameters that can hardly reflect the changes of the remaining system parameters that are not included in the nomograms. The nomograms are based on the linear approximation of the operating limits. These and other considerations introduce conservatism in the "worst case" nomograms in order to robustly cover these uncertainties and inaccuracies. These conservative limits adversely affect the definition of congestion costs on the one hand, and do not completely exclude system problems on the other hand. These circumstances create opportunities for using the real time data including the PMU and EMS/SCADA data to improve and supplement the existing nomograms. These measurements could conceptually validate the existing nomograms in the following ways:

Detection of potential "holes" in the existing nomograms (Figure 1) - The real-time monitoring of the system conditions could help to detect potential situations where the existing nomograms are not capable of detecting system problems. The feasibility of this real-time functionality strongly depends on the observability of system states and parameters needed for this task (this is why a combination of EMS/SCADA and PMU data may be required), and the time resolution of the data required to capture dynamic processes in the system.

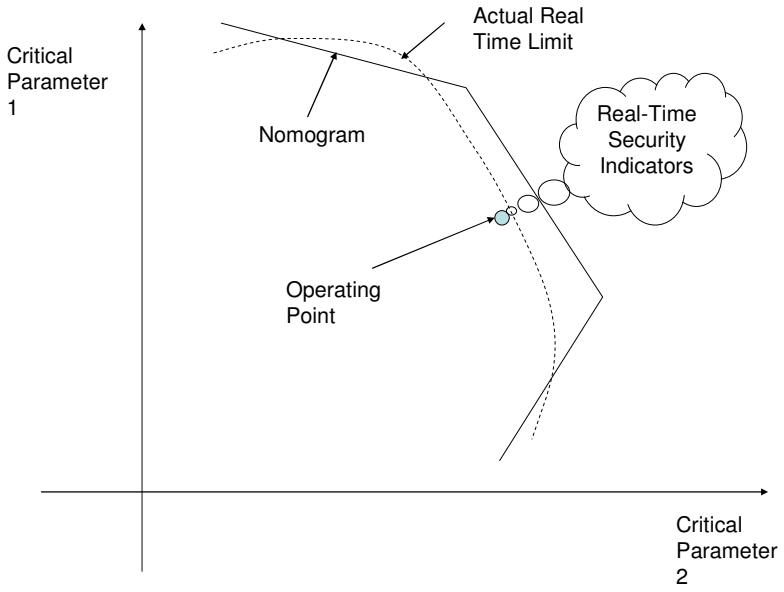

Figure 1: Detecting potential "holes" in the nomograms

Detection of excessive "conservatism" in the existing nomograms - This feature can help to detect potential situations where the existing nomograms are excessively limiting. The elements of this approach can be described as follows (see Figure 2):

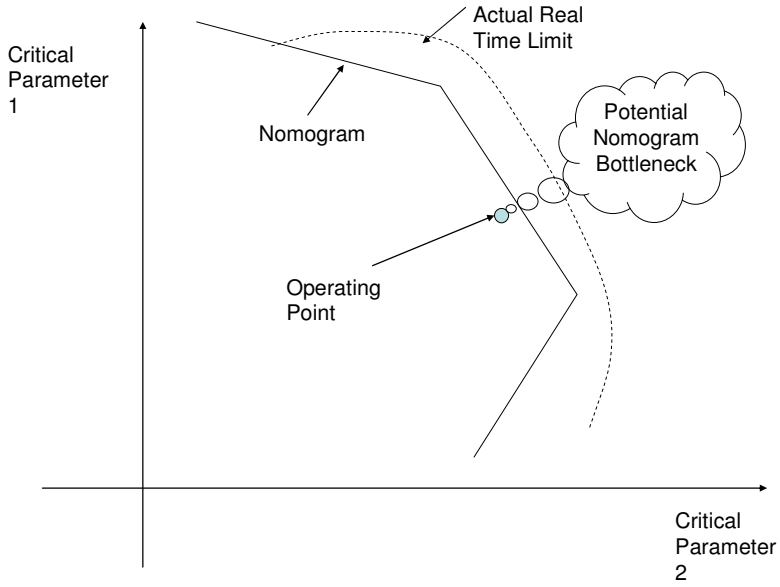

Figure 2: Detecting excessive "conservatism" in the nomograms

The essential elements of the proposed approach can be described as follows:

- At the current operating point, monitor the system security indicators[2] using the PMU, SCADA, and State Estimation data. These indicators can be thermal limits, voltage limits, or other stability indices.
- Monitor the relative position of the current operating point against the "walls" of the relevant nomogram.
- Generate signals to the real-time dispatchers whenever (i) the real-time security indices indicate approaching limiting conditions – i.e. potential "hole" in the nomogram (ii) the operating point reaches the nomogram walls – i.e. potential conservatism in the nomogram.
- Memorize the snapshot whenever the security indicators signal the problem before a vicinity of the nomogram boundary is reached. This information can be used offline to "repair" the pre-calculated nomogram.

[2] Under the current CEC-CAISO Project Plan, the various new stability metrics that are planned for research and development under the "Monitoring" and "Small-Signal Stability" tasks could be used as stability indicators here.

Note: It is important to use this information with caution, because the current operating condition can be very different in comparison to the "worst case" condition implied by the nomogram. The nomogram "repair" should be only authorized when sufficient statistical data has been gathered to indicate the need for this change. The measurement data needs to be augmented with contingency computations based on this data in order to be applicable to updating nomogram walls that account for n-1 security under contingencies.

For local limit assessment purposes, additional PMU units could be recommended to be installed in certain critical locations to provide full observability of the known problem regions so that all the critical and most influential set of parameters and states can be evaluated in real time with very high resolution. In existing systems, the information on possible violations becomes available to the grid operator with resolution from several seconds (within the SCADA/EMS cycle) to several minutes (as a result of the State Estimation cycle). Even if the nomogram monitoring feature is available to the real-time dispatchers at all, the existing systems may have delays that may be critical in some emergency conditions. Sudden unanticipated changes (for instance, the ones that may be precursors of an approaching blackout) and other rapid dynamic processes are hard to capture on time frames based on the SCADA or EMS information. Short-term parameter trends, which could lead to instabilities, and which are so important for predicting violations and real-time decision making, are almost impossible to identify in the existing systems.

The use of PMUs to monitor existing nomograms would help to provide a tighter real-time monitoring of the operational limits. The sub second information from the problem area would increase the situational awareness of the real-time dispatch personnel and allow for more time for timely manual and automatic remedial actions in the future (Figure 3).

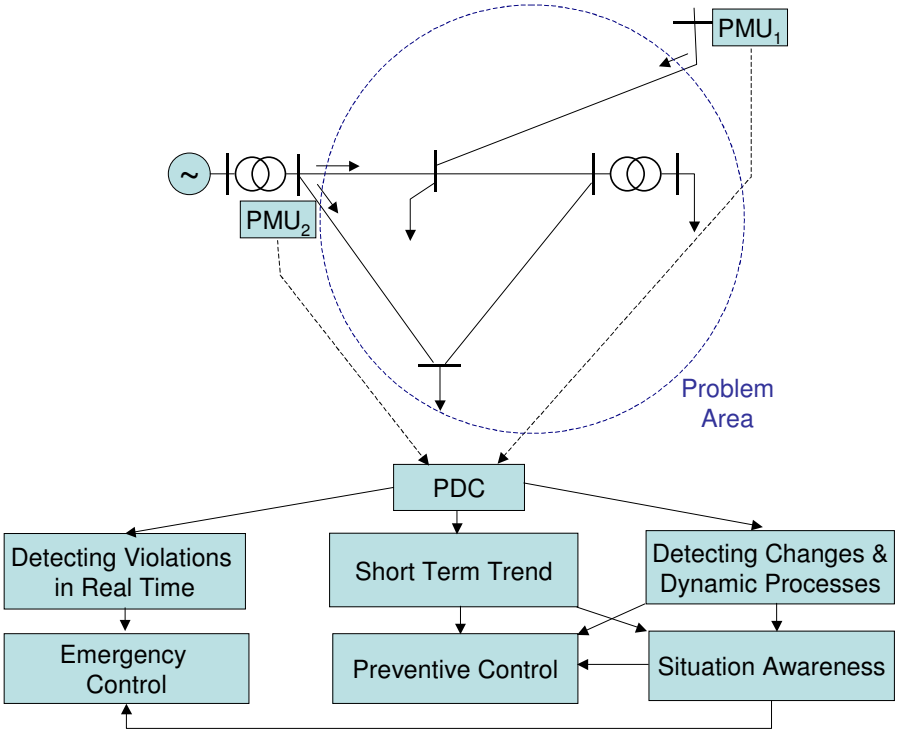

Figure 3: Use of additional PMUs to monitor existing nomograms in real-time

2.2. Use of PMUs for Reduced Dynamic Equivalents and Transient Stability Assessment

Although phasor measurements cannot describe the complete system dynamics they seem to be well suited to identifying reduced dynamic equivalents. Here, a reduced dynamic model designed to capture some aspect of the system dynamics is assumed and the phasor measurements are used to estimate the current parameters of the reduced dynamic model in real time.

For example, the simplest dynamical equivalent is the swing equation for a single machine infinite bus system. With phasor angle measurements from a pair of critical points across the grid, the dynamics of the difference of the two angles can be used to fit the swing equation parameters such as synchronizing and damping torque. This swing equation would capture an aspect of the dynamics between the two areas in which the measurements were taken. Measurements could also be used to identify more elaborate multi-machine dynamic equivalents that would better capture aspects of the western area dynamics. One approach would be to combine together phasor angle measurements in one area to obtain a combined phasor angle measurement representing a lumped node in the reduced dynamic mode representing that area.

These reduced dynamic equivalents may be used in both in transient stability and small-signal oscillatory stability studies. For transient stability, the method relies on identifying a group of machines that separate from the other machines given a particular contingency. The machine groups are assumed to swing together. Consider phasor measurements from two groups - one inside the separating group of machines and one outside the separating group. These two groups of phasor measurements could be used to identify the parameters of the single machine equivalent in the pre-fault system. The change between the fault-on and pre-fault systems could be determined by offline simulation. The same change applied to the measurement based prefault system can be used to obtain an estimate of the fault-on system trajectory. Such a transient stability assessment could be usefully applied to studied patterns of transient stability that cause known separations and to the binding transient stability limits. For oscillatory stability, such reduced dynamic models may capture the low frequency oscillatory modes. An advantage of such a model-based approach is that it may be used to quickly obtain corrective measures to suppress oscillations or increase their damping.

Note: The use of the reduced dynamic equivalent is limited by the extent to which a simpler reduced dynamical model can usefully approximate the entire dynamics. However, in general, the assumption of a dynamic model allows for fewer measurements than in a static model because dynamic observer methods become feasible.

2.3. New Concept of Wide Area Nomograms

Although the existing set of PMU measurements do not provide complete system observability, they could nevertheless provide wide-area visibility and one could conceptualize a completely new type of Wide-Area Nomograms for monitoring. The proposed concept relies on the hypothesis that for these wide-area nomograms, nodal voltage angles (or magnitudes) may provide a more convenient coordinate system for measuring certain stability margins when compared with nodal power injections that are traditionally used for this purpose. In this case the phasor measurements would be ideal candidates for monitoring system conditions with respect to these wide-area nomograms. A frequently proposed simple form of the wide-area nomograms consists of inequalities applied to the voltage angle differences measured at different locations within the Interconnection – see Figure 4.

$$\delta_i - \delta_j \le \delta_{ij}^{\max}, \;\; i, j = 1, 2, 3, ..., n \tag{1}$$

It is intuitively clear that large angle differences indicate more stress posed on the system, and that there are certain limits of this stress that make the system unstable or push it beyond the admissible operating limits such as thermal or voltage magnitude limits. At the same time, conditions applied to the angle differences are quite primitive and do not provide an acceptable accuracy of approximation of the power flow stability boundary, especially due to the nonlinear shape of this boundary.

The most convincing argument for using angles for the nomogram coordinates instead of the more traditional power flows (e.g. interface flows, total generation, total load, etc) is that angles are a more direct measure of transient stability, and therefore better coordinate system for observing transient stability. In particular, the implications of any topology changes, such as line outages, are directly observable in the angle measurement which may otherwise be absent in the MW flows – the angle difference across the interface increases when a line opens while the net MW flows through a corridor may remain unchanged (i.e. the excess power is rerouted through the other parallel lines). For this very reason, while the boundaries of conventional nomograms need to be adjusted to reflect topology changes, the boundaries of nomograms in the new angle coordinate system may be more static and consequently prove to be a more appropriate for monitoring and assessing proximity to instability.

The above mentioned scenario is illustrated by actual event that occurred on June 18th 2006, when a Malin-Round Mountain transmission line outage occurred which redirected the net power flow through the other two lines (Malin-Round Mountain 2 & Captain Jack-Olinda) that collectively define the California Oregon Interface (COI) path. The net COI flows, however, remained unchanged.

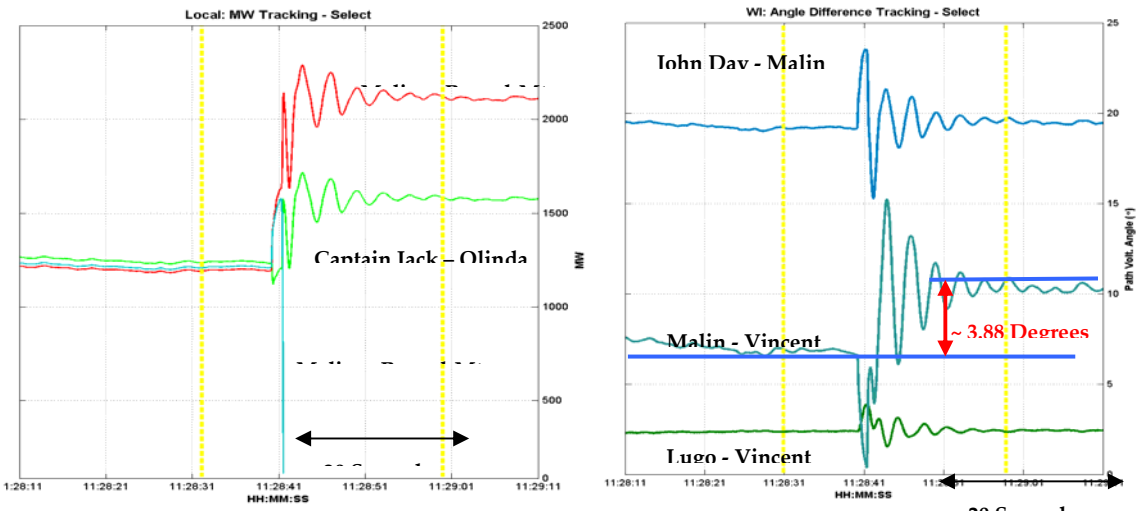

(a) (b)

Figure 4: MW Flow and Angle Difference tracking across COI – (a) the net MW flows remained unchanged (b) the transmission outage was captured by angle difference.

Note: Net MW flow across COI before event = (1207 + 1190 + 1235) = 3632 MW

Net MW flow across COI after event = (0 + 2123 + 1583) = 3706 MW

The above figures illustrate how net COI power flow did not change after the line trip, but, the phase angle difference across COI changed by 3.88 degrees indicating greater stress.

Additionally, the fact that angle differences at other regions did not change seems to suggest that monitoring these angle difference changes can also be used to indicate the location of the event).

A better approximation of the wide-area nomograms could be achieved by applying more precise approximating conditions representing linear combinations of the voltage angles determined at different locations within the Interconnection. A hypothetical wide area nomogram for three angles (shown in Figure 4) could be described by the following set of inequalities:

$$\begin{cases} \rho_{11}\delta_1 + \rho_{12}\delta_2 + \rho_{12}\delta_2 \le \delta_1^{\max} \\ \rho_{21}\delta_1 + \rho_{22}\delta_2 + \rho_{22}\delta_2 \le \delta_2^{\max} \\ \ldots \\ \rho_{m1}\delta_1 + \rho_{m2}\delta_2 + \rho_{m2}\delta_2 \le \delta_m^{\max} \end{cases} \qquad (2)$$

Figure 5 shows a conceptual view of the simple angle difference nomogram (a) and advanced angle nomogram (b). The angle difference nomogram is basically a set of straight lines corresponding to different levels of δ_3. The advanced angle diagram gives a set of broken straight lines that can be adjusted to provide a better accuracy of the stability boundary approximation. It is clear that the advanced angle nomogram can follow the actual nonlinear shape of the stability boundary much more closely and consequently provides much better accuracy than the simple angle difference nomogram. The advanced angle approach, solely based on the angle differences, is more related to the static angle stability and active power "loadability" of the Interconnection.

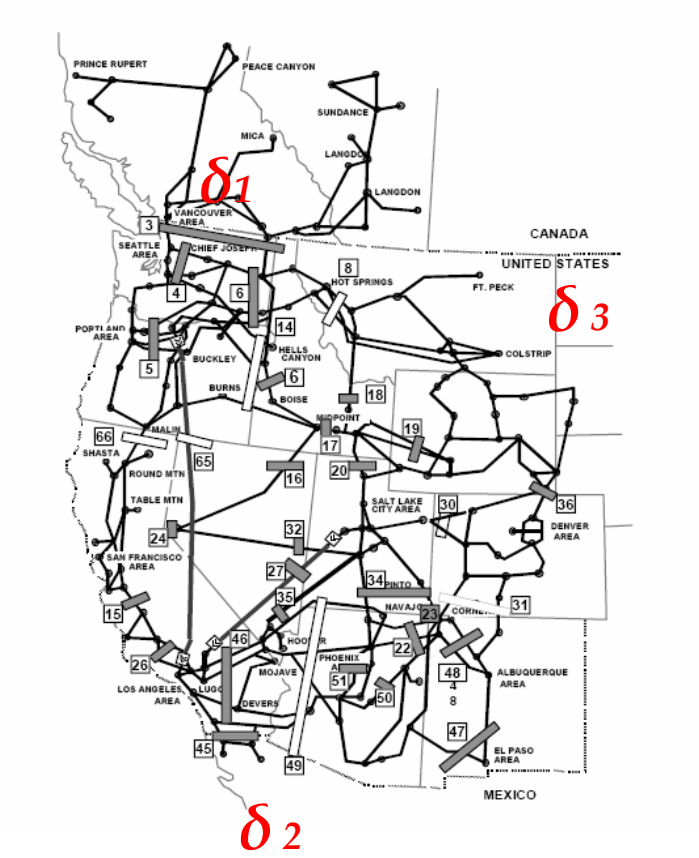

Figure 5: Western interconnection transmission paths

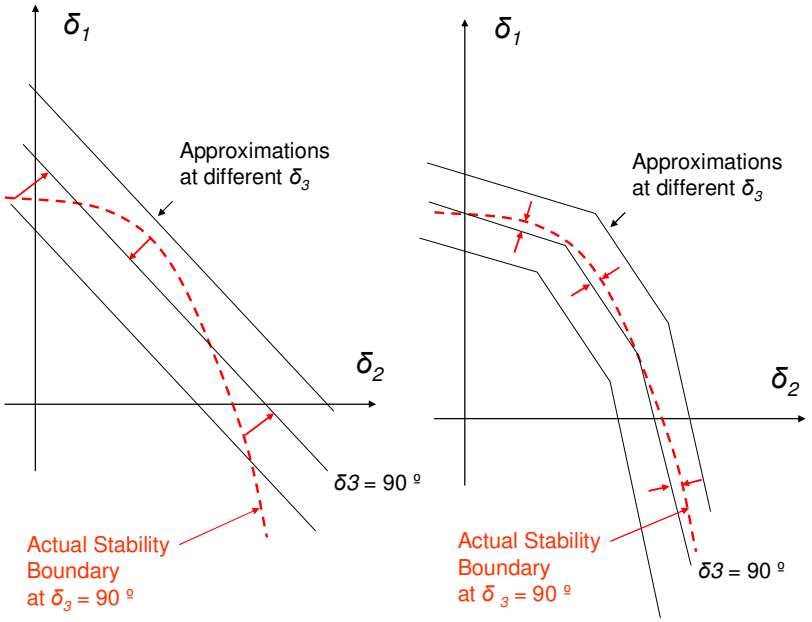

(a) (b)

Figure 6: Conceptual view of simple angle difference and advanced angle nomograms

An even more accurate approximation can be achieved by the use of Cartesian coordinates instead of the polar coordinates, and by the use of m linear combinations of active and reactive components of the nodal voltages measured at different locations 1… n in the system describing the proposed wide-area nomograms:

$$\alpha_{i1}V_1^{'} + \beta_{i1}V_1^{"} + \alpha_{i2}V_2^{'} + \beta_{i2}V_2^{"} + \ldots + \alpha_{in}V_n^{'} + \beta_{in}V_n^{"} \le \gamma_i, \quad i = 1,\ldots,m \tag{3}$$

Numerical experiments with the use of Cartesian coordinates on the test example in Figure 6 show that the stability boundary has a "more linear" shape and consequently is more accurate in its approximation.

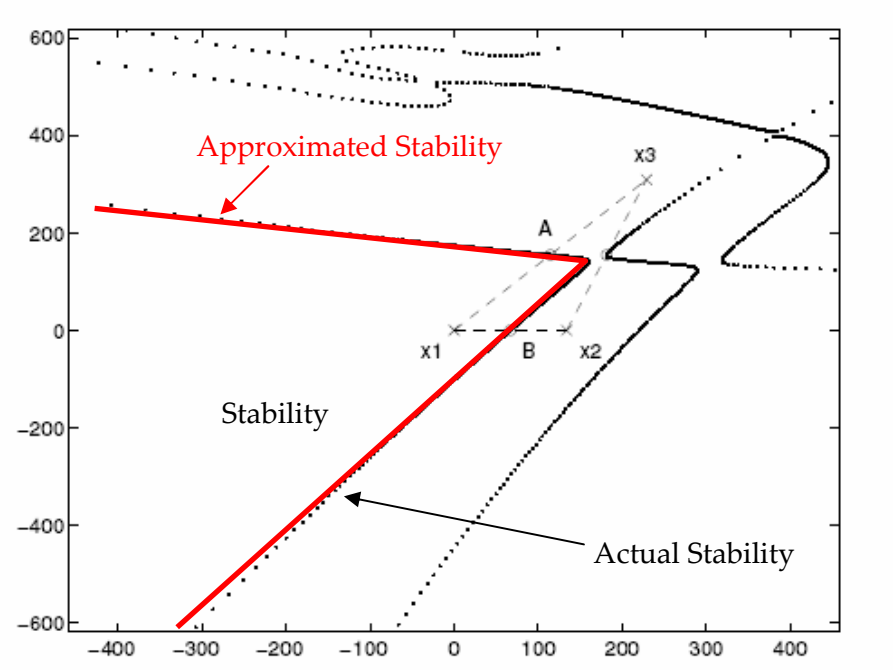

Figure 7: A cutset of stability boundary in rectangular coordinates of nodal voltages (New England test system)[3]

Hence, a new concept of measuring the stability margin by distances calculated in the space of nodal voltages can be suggested.

While angles may be more conducive to monitoring stability, MW flows are still the true controllable variables in the power system. Hence, understanding the relationship between angle differences across a critical interface and MW flows through it is still important. Figure 8 show the net MW imports into California through the California-Oregon Intertie (COI) over a 24 hour period under normal system conditions. Also shown is the angle difference between John Day (a substation up north in Oregon) and Vincent (a substation down south in southern California). The close correlation between these two trends suggest (1) using well chosen angle difference pairs to monitor stability does capture the conventional information present from monitoring the MW path flows while having the added advantage of also reflecting topology changes as mentioned earlier; (2) the relationship between flows and angle differences can easily be ascertained from similar trends - e.g. Figure 8 trends suggest a 15 degree angle change for 1,000 MW increase in COI flows.

3 Y.V. Makarov, V. A. Maslennikov, and D. J. Hill, "Calculation of Oscillatory Stability Margins in the Space of Power System Controlled Parameters", Proc. International Symposium on Electric Power Engineering Stockholm Power Tech: Power Systems, Stockholm, Sweden, 18-22 June 1995, pp. 416-422.

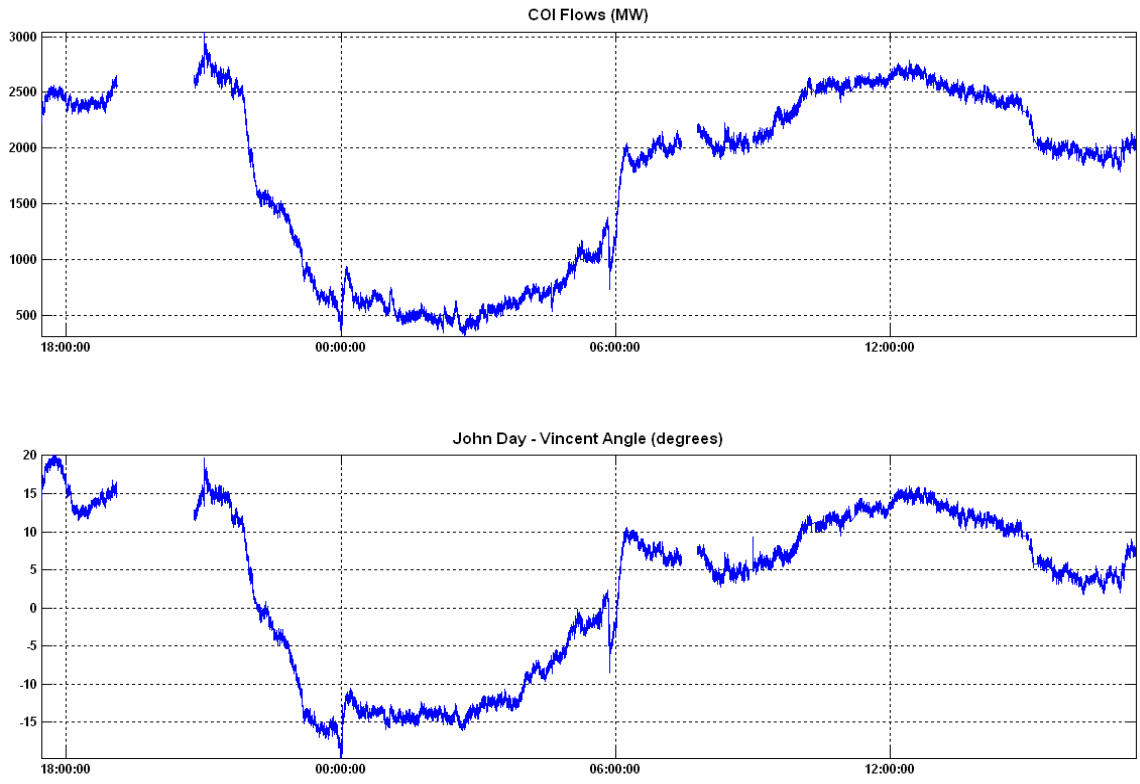

Figure 8: Correlation between MW flows across critical flowgates and angle difference pairs

To better understand the behavior of these nodal voltage angles, these measurements were gathered over several hours by PMUs from different geographic locations within the Western Electricity Reliability Council (WECC) phasor network was used to generate the plots in Figure 9 (a) and (b). Using one of the three nodal voltage angles as the reference, the relative angles at the other two locations was plotted in angle-angle space. In these plots, each set of hourly data is represented by a different color as indicated by the legend. The fact that these trends fall along a narrow and almost linear corridor in this angle-angle space indicates that the behavior of these relative angles is highly correlated with each other. The directionality of this corridor on the other hand is representative of the interdependence of the interaction. For example, if angle differences are indicators of static stress across the grid, then the orientation of the trends in (a) suggests an increase in the stress across one interface implies an increase in the stress across the other interface. However, the trend orientation in (b) suggests the contrary - an increase in the stress across one interface causes the relief of the stress across the second interface. This strong correlated behavior also suggests that limited observability with a few PMUs at key locations may be adequate to capture the system dynamics from a global prospective.

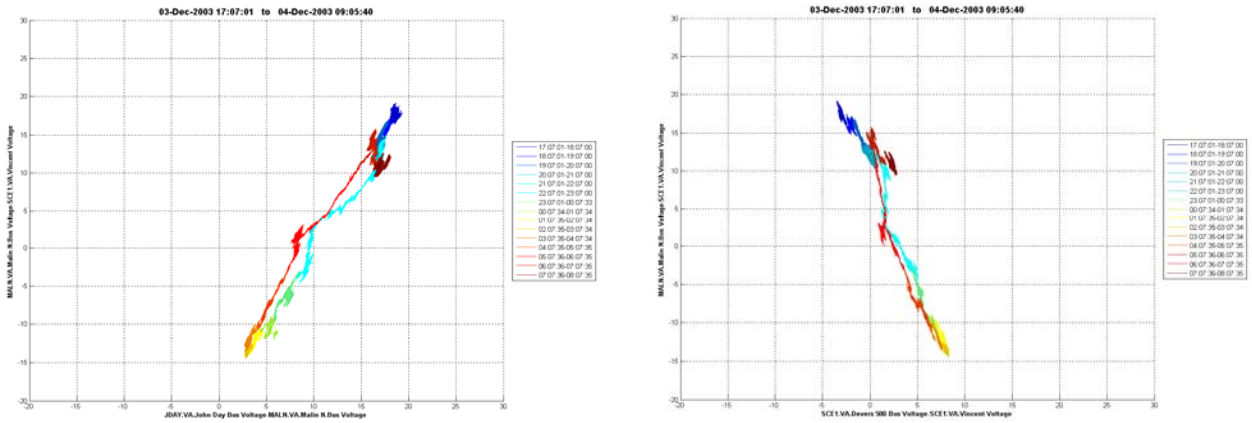

(a) **(b)**

Figure 9: PMU Measurement based phase angle trends in angle-angle space

2.4. Use of PMUs for Wide-Area Voltage Security Assessment

A California PIER funded parallel effort by Consortium for Electricity Reliability Technology Solutions (CERTS) is currently underway in developing a Voltage Security Application (VSA) that runs in real time and provides real time dispatchers with real time reliability metrics related to voltage stability limits. The VSA application under development will be linked to the CAISO EMS system model and data. It will be used to develop and approximate voltage security regions (a type of multi-dimensional nomograms) using linear approximations or hyperplanes, calculate voltage stability indices. In addition, VSA will identify and display abnormal low voltages, weak elements and places in the system most vulnerable to voltage and voltage stability related problems. This application will also perform contingency analysis and provide the system operators with contingency rankings based on voltage problems for the purposes of system monitoring and selecting preventive and emergency corrective actions.

The VSA platform described above can easily be expanded to study wide-area voltage stability problems by selecting global stressing directions and developing the corresponding security regions. The algorithms being developed in the VSA application provide voltage magnitude and angle information, as well as their corresponding sensitivities and participation factors in voltage collapse. Hence, while the proposed VSA framework uses data from the CAISO state estimator and assumes full observability, this same VSA framework could also be used to develop wide-area nomograms whose coordinates would be nodal voltage magnitudes and angles, and the PMU measurements could directly be used to monitor the system conditions with respect to these new nomograms for a wide-area security assessment (Figure 10).

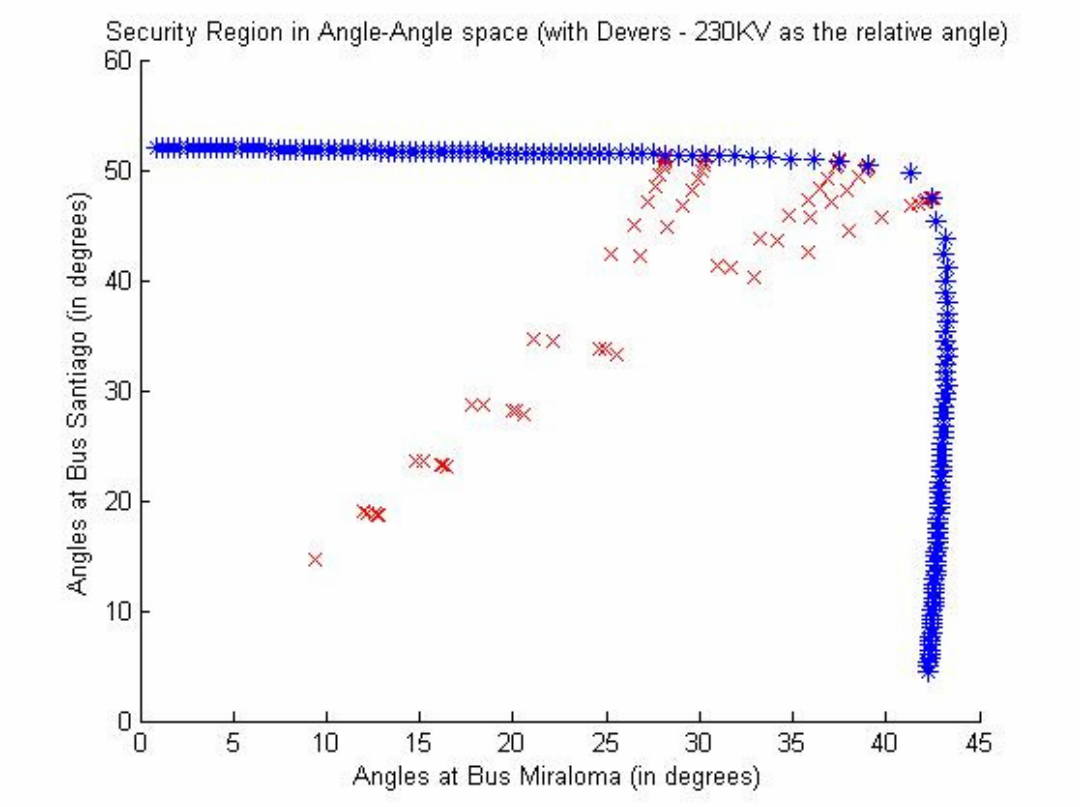

Figure 10: Voltage stability boundary developed in angle-angle space

2.5. Augmenting Existing Nomograms using Small-Signal Stability Assessment

Although small signal stability models and analysis tools are not widely used in the Western Interconnection, there is a growing interest to better understand small-signal stability limits and possibly build associated nomograms for the WECC system. This is based on the observation that some types of potential instabilities could manifest themselves ahead of time through growing oscillations observed in the system. For example, it has been noticed that insufficient frequency response in California could lead to changes of the power flow patterns in post-transient conditions and may lead to additional limits of the Operating Transfer Capability (OTC) on the Oregon-California interties. The nature of these limitations is related to growing oscillations. The low frequency oscillations observed in the system are consequently of interest because they characterize the stability of the power system and limit the power flow across regions. While there is a danger that such modes can lead to instability in the power system following a sizable event in the system, there is also the risk of these modes becoming negatively damped or unstable due to gradual changes in the system. The ability to continuously track these modes and assess their stability would therefore be a valuable tool for power system engineers. Fortunately, the high resolution and wide-area visibility that PMUs offer are well suited to observe these modes and assess the damping associated with these low frequency modes in real-time.

Small-signal stability software can be an essential addition to the real-time monitoring capabilities offered by PMU measurements. State estimation results coupled with small signal stability models can help to identify the origin of poorly damped oscillations. The identification of oscillatory parameters such as magnitude, damping and frequency are needed before one can select measures to increase the stability margin.

The PMU snapshot data recording can be activated by poorly damped oscillations registered by PMUs and identified by the Small-Signal Stability Monitoring applications. Parameters of these oscillations such as frequency, magnitude, and damping can be identified using special algorithms. Subsequent offline analysis using small-signal and transient stability models will reveal how close these models are to reality. The use of offline models will help to better understand the origin and nature of these oscillations. Questions such as what changes in the system cause oscillations and the identification of a small set of descriptive variables that capture the phenomena are also some of the central issues related to the existing modal analysis tools.

Research work could be conducted to investigate the validity of such an approach. The objective of this study could be to screen the WECC system for locations where the Operating Transfer Capability (OTC) is limited by oscillatory problems. Then the typical frequencies could be determined. The next step is to find the places where these oscillations are better observable, and associate these locations with PMU placement. Oscillation-related OTC limits could be compared with the existing nomograms, or may indicate the necessity of building additional nomograms. After such a set of verification and validation procedures, the results of the PMU-based modal analysis could be used to detect potential violations in real time. Finally this will lead to the improvement of the pre-calculated nomogram limits based on real-time PMU data by observing the differences between the pre-calculated OTC and the real transfers at which the oscillations start to grow.

3.0 ALGORITHMS FOR MONITORING SMALL-SIGNAL STABILITY WITH PHASOR MEASUREMENTS

The underlying assumption enabling swing-mode estimation is that the power system is primarily driven by random processes when operating in an ambient condition. An ambient condition is one where there is no significant disturbance occurring within the system. The primary driving function to the power system is the random variations of the loads. It has been shown that under such an assumption, the resulting power-system signals will be colored by the system dynamics. This coloring allows one to estimate the swing-mode frequencies and damping terms.

Consider the signal flow diagram in Figure 11 representing the excitation of a power system from random load variations. $\underline{v}(t)$ is a vector of random components added to each load; each element independent of the other. The output $y_i(t)$ is the ith measured signal at time t, and $\mu_i(t)$ is measurement noise located at the transducer. In general, $\mu_i(t)$ is a relatively small effect when quality instrumentation is employed; therefore, its effect is often negligible. Theory tells us that because $\underline{v}(t)$ is random, each $y_i(t)$ will also be random. But, $y_i(t)$ is colored by the dynamics of the system.

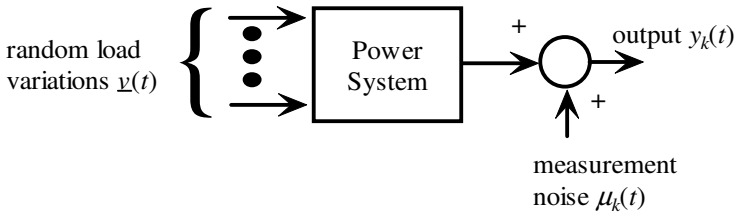

Figure 11: Signal flow diagram.

Assuming a linear system mode, the output y_i from Figure 11 can be written in auto-regressive moving-average (ARMA) form as

$$y_i(kT) = \sum_{j=1}^{n} a_j y_i(kT - jT) + \sum_{l=1}^{p} \left(\sum_{j=0}^{m_{il}} b_{ilj} v_l(kT - jT) \right) + \mu_k(kT),\ i = 1, 2, \ldots, n_o \quad (4)$$

where n_o is the number of output signals measured, T is the sample period, k is the discrete-time integer, n is the order of the system, p is the order of vector $\underline{v}$, and m_{il} is the MA order of the ith output for the lth input. The autocorrelation of y_i is defined to be

$$r_i(q) = E\{y_i(kT) y_i(kT - qT)\} \quad (5)$$

where $E\{\bullet\}$ is the expectation operator. Over a finite number of data points, the autocorrelation is approximated by

$$r_i(q) \cong \frac{1}{N}\sum_{k=q+1}^{N} y(kT)y(kT-qT) \tag{6}$$

where N is the total number of data points. Using the same analysis in [1], it can be shown that the autocorrelation satisfies

$$r_i(q) = -\sum_{j=1}^{n} a_j r_i(q-j)\,,\ q > m \tag{7}$$

where $m = \max(m_{il})$. Another useful relationship involving the autocorrelation is

$$S_{ii}(\omega) = F\{r_i(q)\} = E\{Y_i(\omega)Y_i^*(\omega)\} \tag{8}$$

$$r_i(q) = F^{-1}\{S_{ii}(\omega)\} \tag{9}$$

where $F\{\bullet\}$ is the Fourier transform operator, $Y_i(\omega)$ is the Fourier transform of $y_i(t)$ at frequency ω, and $Y_i^*(\omega)$ is the conjugate of $Y_i(\omega)$. S_{ii} is termed the power spectral density (also referred to as the autospectrum) of y_i. Effectively, it represents the energy in a signal as a function of frequency. If one knows the Auto-Regressive (AR) a_j coefficients in (4), then the system poles (or modes) can be calculated from the following equations.

$$z_j = roots\left(z^n + a_1 z^{n-1} + \ldots + a_n\right),\ j = 1, 2, \ldots, n \tag{10}$$

$$s_j = \frac{\ln(z_j)}{T} \tag{11}$$

3.1. Algorithms to Estimate the System Modes Using Synchronized Phasor Data

Estimating a power system's electromechanical modal frequency and damping properties using ambient time-synchronized signals is achieved by using parametric system identification methods. Three estimation algorithms to solve the AR coefficients and thus the system modes have been well studied for application purposes and they are:

- Modified extended Yule Walker (YW),
- Modified extended Yule Walker with spectral analysis (YWS), and
- Sub-space system identification (N4SID).

(1) Modified Extended Yule Walker (YW)

The original Yule Walker algorithm is used to estimate the AR parameters and thus the system poles. The extended modified Yule Walker (YW) algorithm is a modified version of the original Yule Walker algorithm with extension to multiple signals for the analysis of

ambient power system data, namely, frequency data, voltage angle data, and etc. The algorithm starts by expanding (7) into matrix form as

$$\begin{bmatrix} r_i(m) & r_i(m-1) & \cdots & r_i(m-n+1) \\ r_i(m+1) & r_i(m) & \cdots & r_i(m-n+2) \\ \vdots & \vdots & \ddots & \vdots \\ r_i(m+M-1) & r_i(m+M-2) & \cdots & r_i(m+M-n) \end{bmatrix} \begin{bmatrix} a_1 \\ a_2 \\ \vdots \\ a_n \end{bmatrix} = - \begin{bmatrix} r_i(m+1) \\ r_i(m+2) \\ \vdots \\ r_i(m+M) \end{bmatrix} \tag{12a}$$

or

$$R_i \underline{a} = -\underline{r}_i \tag{12b}$$

For each output, (12) can be concatenated into one matrix problem as

$$\begin{bmatrix} R_1 \\ R_2 \\ \vdots \\ R_{n_o} \end{bmatrix} \underline{a} = - \begin{bmatrix} \underline{r}_1 \\ \underline{r}_2 \\ \vdots \\ \underline{r}_{n_o} \end{bmatrix} \tag{13}$$

The steps for solving the YW algorithm involve

- Estimating autocorrelation terms using (6),
- Constructing autocorrelation matrix equations (13),
- Solving the equations (13) for the AR coefficients,
- Solving the coefficients equation (10) for the discrete-time modes, and
- Converting the discrete-time modes to the continuous-time modes using (11).

(2) Modified Extended Yule Walker with Spectral Analysis (YWS)

The modified extended Yule Walker with Spectral analysis (YWS) follows the same procedure as the YW method to estimate the system modes, i.e., that the system modes are solved from AR coefficients which in turns are solved from the system autocorrelation matrix equations. However, the YWS algorithm estimates the system autocorrelation terms from its spectrum (9), while the YW algorithm estimates the system autocorrelation terms directly from data samples (6).

(3) Sub-Space System Identification (N4SID)

The third algorithm considered for mode estimation is the time-domain subspace state-space system identification algorithm known as N4SID. The reader is referred to [2] and [3]. Application of the N4SID algorithm to ambient power system data is described in [4]. The algorithm used for this report is implemented in the Matlab function "n4sid" available with the system identification toolbox. Because of the complexity and length of the

algorithm, it is not repeated here. Similar to the YW and YWS algorithm, the N4SID algorithm provides an estimate of the system's characteristic equation parameters.

3.2. Mode Selection

When applying the previous mode estimation algorithms, one ends up estimating many "extra" modes due to numerical over fitting. A fundamental problem is determining which of the modes are actually contained in the system and which are numerical artifacts. This problem is addressed by developing a method of calculating the most "dominant" modes in a signal. The dominant modes are then judged to be the ones contained in the system.

Because the signals are random, one cannot directly calculate the energy of a given mode within the signal. But, one can estimate the "pseudo energy" of a given mode within the autocorrelation function. If one takes the Z-transform of the equation (7) and solves for $r_i(q)$ in parallel form, one obtains

$$r_i(q) = \sum_{j=1}^{n} B_{ij} z_j^{q-m-1}, \; q > m \tag{14a}$$

where z_j is the jth discrete-time pole, and B_{ij} is termed the residue for pole z_j and output i referenced to time m+1. This is expanded into matrix form as

$$\begin{bmatrix} z_1^0 & z_2^0 & \cdots & z_n^0 \\ z_1^1 & z_2^1 & \cdots & z_n^1 \\ \vdots & \vdots & \ddots & \vdots \\ z_1^{M-1} & z_2^{M-1} & \cdots & z_n^{M-1} \end{bmatrix} \begin{bmatrix} B_{i1} \\ B_{i2} \\ \vdots \\ B_{in} \end{bmatrix} = \begin{bmatrix} r_i(m+1) \\ r_i(m+2) \\ \vdots \\ r_i(m+M) \end{bmatrix} \tag{14b}$$

Equation (11) can is solved for the unknown B_{ij} terms. The "pseudo mode energy" of mode j in signal i is then defined to be

$$E_{ij} = B_{ij}^* B_{ij} \sum_{q=0}^{M-1} \left[\left(z_j^q \right)^* \left(z_j^q \right) \right] \tag{15}$$

To select estimate a mode in a signal, the following steps are conducted:

- One of the three algorithms (YW, YWS, or N4SID) is used to estimate the system modes (z_i, i=1,…,n for discrete-time; s_i, i=1,…,n for continuous time).
- The pseudo modal energies are calculated by solving (14) in a least-squares sense and (15).
- The modes within a specified region of the s-plane are saved and ordered according to their energy.

3.3. Algorithm Tuning

To use each of the algorithms, several analysis parameters must be selected. This includes all the parameters in equations (4) through (15).

- N = number of data points used for analysis (required for all algorithms). Note that T_{total} = $T*N$.
- T = sample period for collecting data (required for all algorithms).
- n_o = number of signals to analyze (required for all algorithms).
- n = model order (required for all algorithms).
- m = MA order (required for YW, YWS, and mode selection algorithms).
- M_{AR} = number of samples of the autocorrelation function used to solve for the AR parameters. This equal to M in equation (9a). Required for the YW and YWS algorithms.
- N_{fft} = number of samples used for the *pwelch* function in YWS.
- M_{RES} = number of samples of the autocorrelation function used to solve for the residue parameters. This equal to M in equation (10b). Required for the all three algorithms.

Extensive research on how to select these parameters has been done [5]. The research includes testing and evaluating the algorithms by Monte-Carlo simulations on a test system as well as analysis of WECC PMU data. The recommended analysis parameters from the research are:

T = 0.2 sec.

T_{total} = 5 minutes or greater

n_o = 1 to 4 signals

n = 25, m = 10 for YW and YWS.

n = 20, m = 5 for N4SID.

M_{AR} = M_{RES} = 10 sec.

The above algorithms were applied to western system data. Approximately 2 hours of ambient data was collected from several PMUs within the WECC system on March 7, 2006. Extensive spectrum analysis was conducted on the data to determine the modal content. Analysis of the data indicated that frequency error estimated from finite-difference of the voltage angles provided quality data.

Table 1 summarizes the results from the spectral analysis. As typical of the WECC system with Alberta connected, the system is dominated by the 0.265-Hz "Intertie" mode and the 0.385-Hz "Alberta" mode. Several higher-frequency weaker inter-area modes are also described in

Table 1.

The first step in the modal analysis is to select the appropriate signals. The goal is to select signals with high observability (i.e., large peaks in the power spectrum) of the "Intertie" and "Alberta" modes and low observability of the other modes. This is most easily done by

subtracting two signals that oscillate out of phase from each other at the frequencies of interest. Scanning

Table 1, one sees that the following signals are excellent choices for estimating the two modes of interest:

- (Grand Coulee Handford) – (Big Creek 3 230kV)
- (John Day) – (Vincent 230kV)

The 10 min. analysis window was applied to just over two hours of ambient data by sliding it in 5 min. steps. This results in 25 total mode-meter analyses. For each case, the two modes with the largest pseudo-energy terms in the region of the s-plane bound by 0.2 Hz, 0.5 Hz, and 20% damping were estimated with a mode-meter algorithm. The s-domain plots of the results are shown in Figure 12. The two dominant "Intertie" and "Alberta" modes are observable within this data set and shown on the plots. All three algorithms are able to identify these modes with consistent results and comparable performance. Additionally, while the modal frequencies are relatively constant over the entire duration of the data set, there appears to be much greater variability in the % damping (i.e. 5% - 20% damping) over time. Additionally, a longer term (24 hours) behavior of the "Intertie" mode (frequency & damping) and corresponding California-Oregon Intertie (COI) loading conditions for different is shown in Figure 13. This plot shows a great deal of variability in the % damping over the 24 hour period.

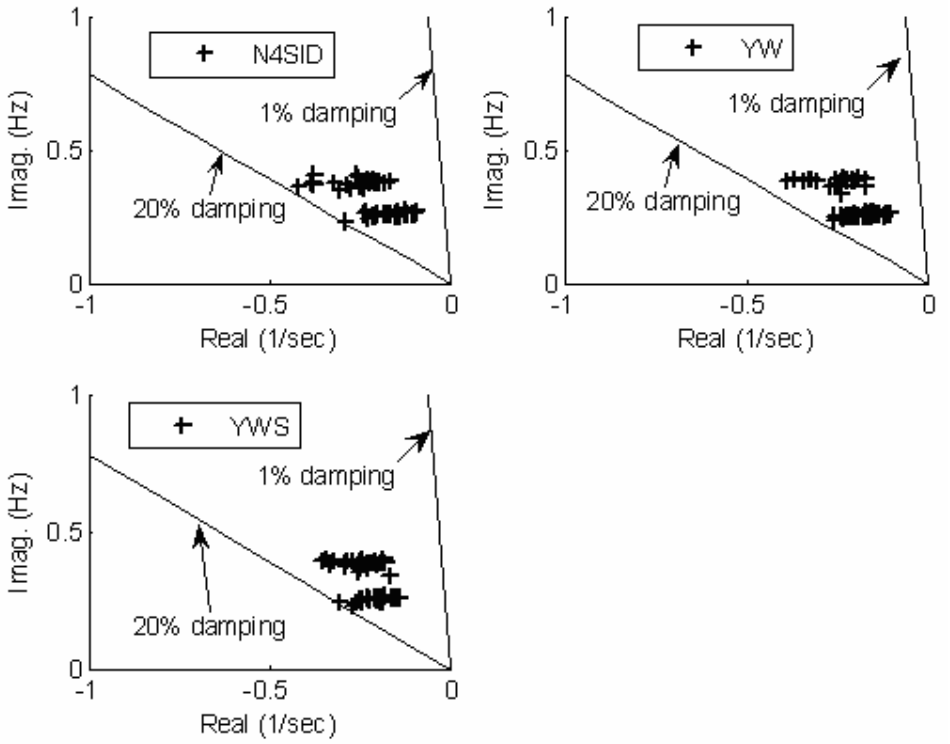

Figure 12: Mode estimates for WECC data

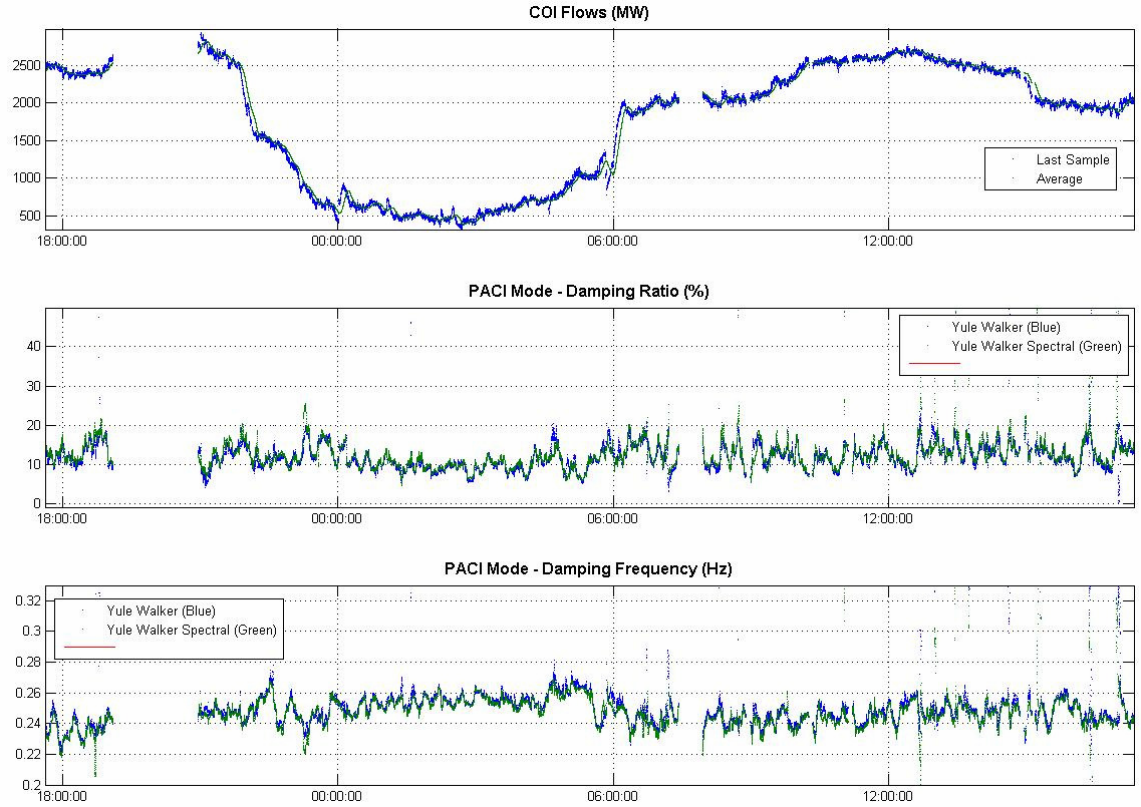

Figure 13: Long-term Intertie mode trends (frequency & damping) with varying COI flows

Furthermore, in addition to the modes estimation algorithms discussed above, it is also desirable to understand the observability of a mode at a particular monitoring location. Such information will be helpful in identifying appropriate points for control actions towards mitigating poor damping situations. Waterfall plots, which are series of power-spectrum snapshots of a monitored signal over time, are important for such investigation. The waterfall plot for the COI flows over the latter half of 24 hour period is shown in Figure 14, where the power-spectral density within the frequency range of interest (y-axis) and its recent trends over time (x-axis) are illustrated. The magnitude of the power spectra shown along the z-axis (color-coded) truly indicates the power inherent in the selected signal and is interpreted as the square of the rms of the magnitude of the components in the signal along the frequency axis. Note that the variability observed in the % damping at 0.25 Hz (Figure 13) is also visible in the power-spectral density at the same 0.25 Hz – i.e. as this mode's damping changes over time, the spectral peak at this modal frequency becomes more/less prominent. Such modal variability over longer term time scales (minutes and hours) needs further investigation.

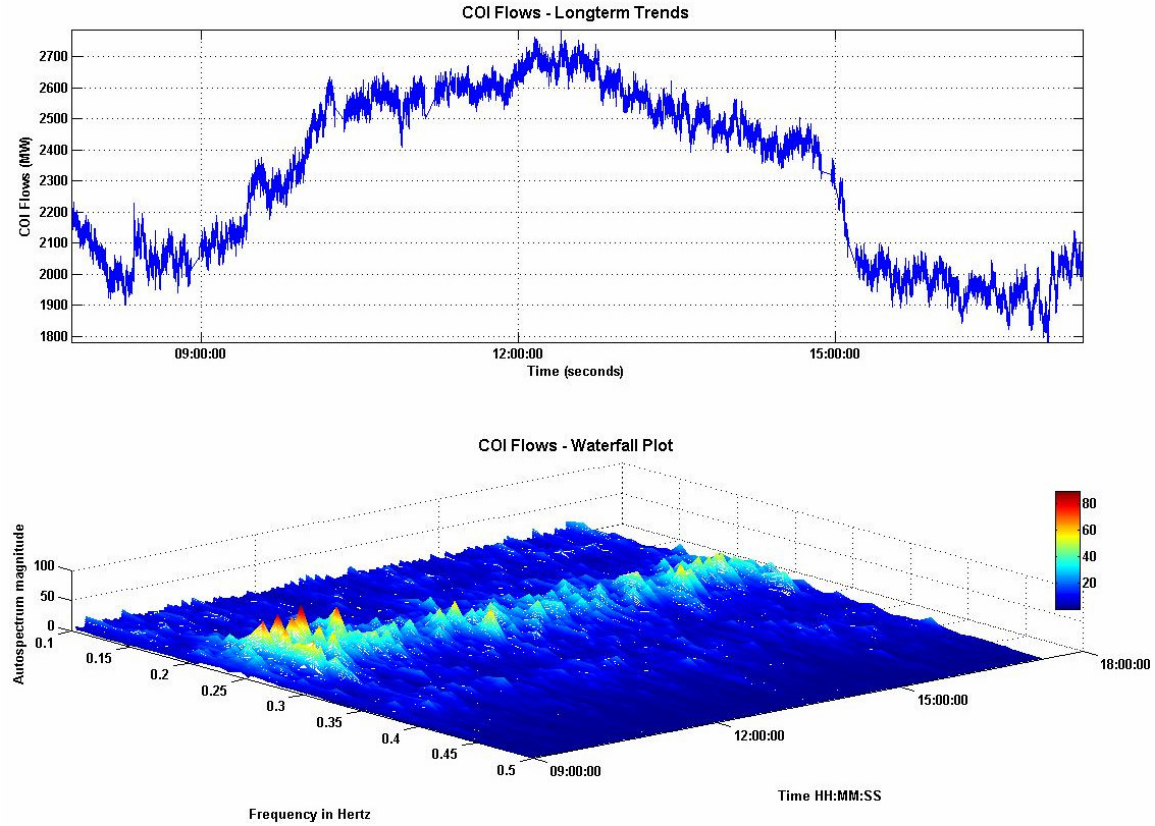

Figure 14: Long-term Intertie mode spectral trends with varying COI flows

3.4. Implementation of Small-Signal Stability Monitoring Prototype Tool

During 2006, a *Small-Signal Stability Monitoring* application that utilizes the above mentioned algorithms to monitor and track the low frequency modes prevalent within the power system in real time and under ambient system conditions, was developed. The application underwent field trial at both the CA ISO and BPA, prior to being migrated onto production hardware and installed in the CA ISO control center in June 2007. A sample operator display from this tool is shown in Figure 15.

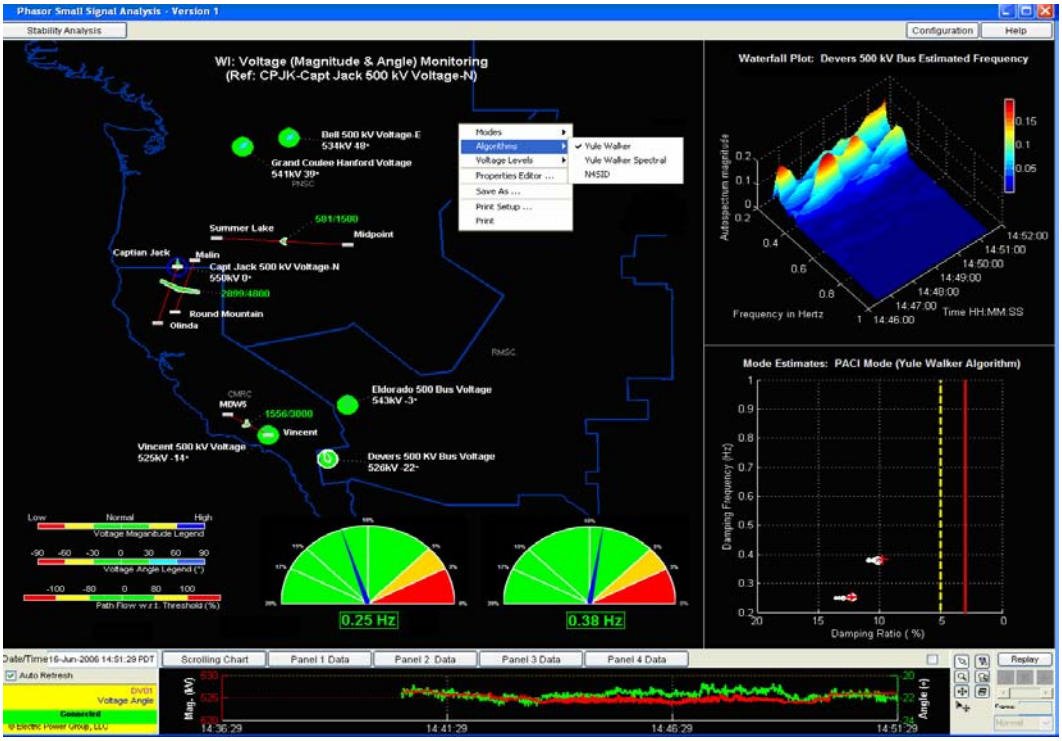

Figure 15: Small-Signal Stability Monitoring Display

Some of the visualization capabilities that are available within the Small-Stability Monitoring tool include:

- Color-coded 'speedometer' type gauges that provide information on damping ratios and damping frequencies of the observable modes in the system. The sub-areas within each gauge are color coded to represent different ranges of damping ratios – i.e., a 5%-20% damping ratio shown in green indicating a safe operating region; a 3%-5% damping ratio in yellow indicating an alert condition; and less than 3% damping ratio shown in red representing an alarm situation. The positions of the needles swing back and forth in real time to indicate the current damping ratios of the system modes.

- Mode tracking plot that offers valuable information on the most recent modal trends to operators (Figure 16). Here the most recent (red crosses) and the historical (white circles) modes are shown within a 2-dimensional Frequency (in Hz) vs. Damping (in %) plane. Hence, the recent damping ratio patterns can be traced by observing the trace of the modes along the horizontal axis on the plot. Similar to the above mentioned mode meter gauges, yellow and red lines set the thresholds for the alert- and alarm-level of damping ratio on the plot.
- Waterfall plot which is a joint time-frequency domain plot and an illustration of the power-spectral density within the frequency range of interest (typically 0.1Hz – 1Hz for inter-area electro-mechanical modes) and its recent trends over time.

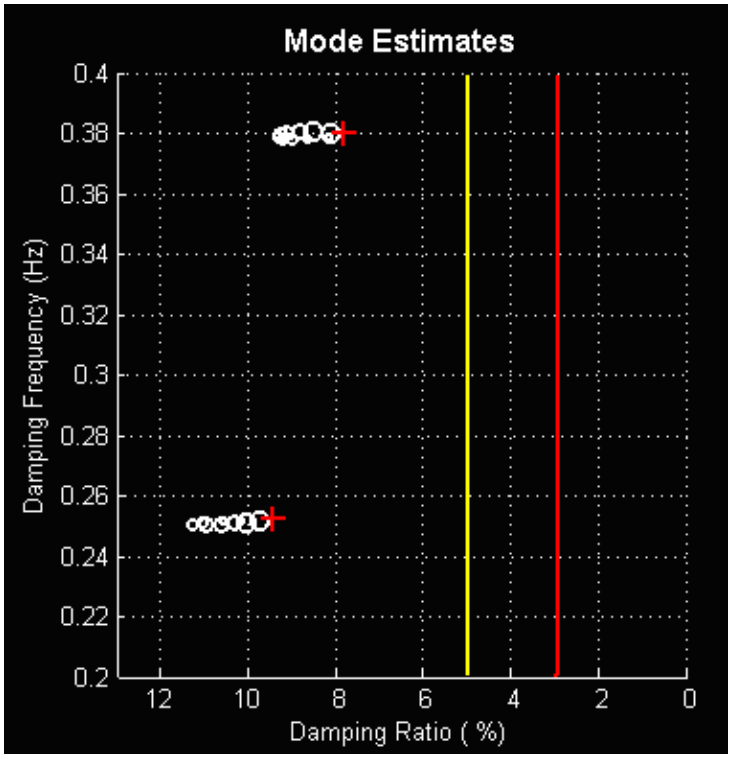

Figure 16: Sample Mode Tracking Plot

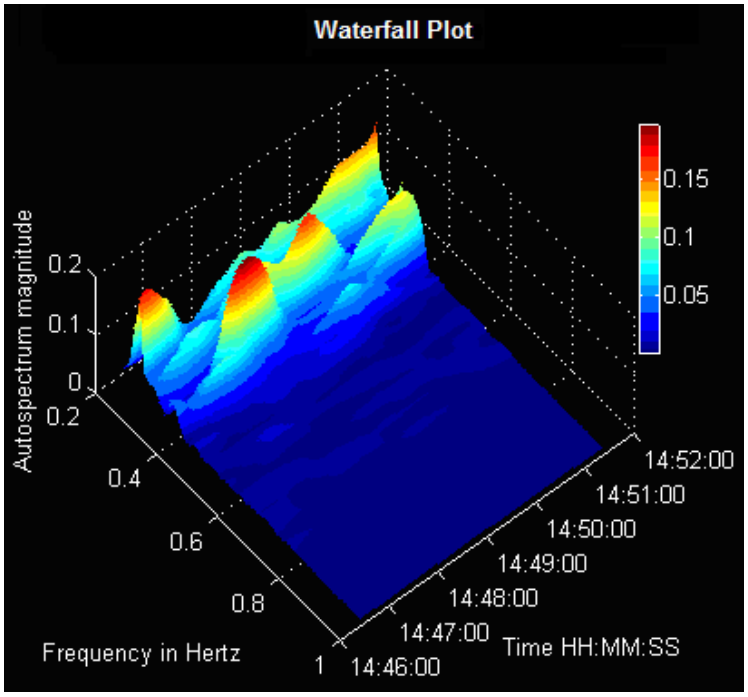

Figure 17: Sample Waterfall Plot

It is important to mention that appropriate pre-processing of the data prior to running the algorithms is critical to performance the tool and the accuracy of the modal estimates. Data pre-processing stage includes removing outlier and missing data, detrending, normalization, anti-aliasing filtering and down sampling, etc. Additionally, to help focus on the interested range of frequency of the modes (i.e., the range of wide-area oscillations), proper post-processing is also desired. Post-processing includes setting the maximum number of modes for display, setting the maximum associated damping ratio, setting the energy threshold for the modes, and setting proper frequency range. These pre- and post-processing stages have been incorporated into the mode the prototype and are end-user configurable (Figure 18).

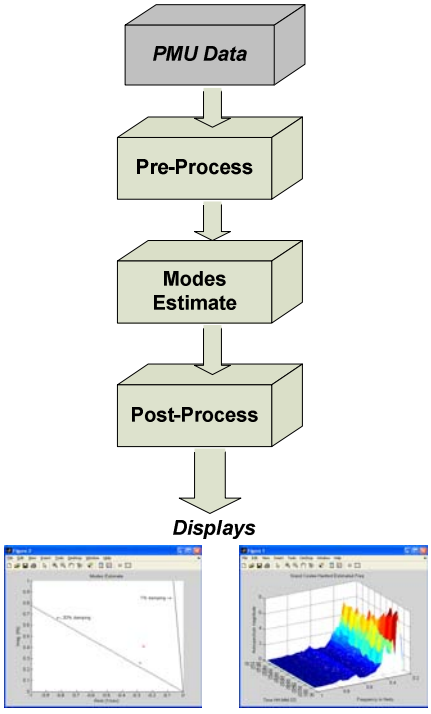

Figure 18: Block Diagram for the Small-Signal Stability Monitoring Tool.

In late 2007/early 2008, the Small Signal Stability tool's algorithms, visuals and feature set were further enhanced based on additional research and end user feedback. Some of the improvements included:

- Improved mode estimation algorithms and graphics to quantify the uncertainty associated with the mode estimates. Here, a newly developed 'bootstrapping' method was embedded into the tool that compute the uncertainty region or error bounds (a.k.a. confidence intervals) associated with each estimate and is illustrated as an ellipse on the same 2-D frequency vs. damping ratio plane representing the uncertainties in both the modal damping and frequency (Figure 19). A smaller ellipse would therefore signify greater confidence in the modal estimate while a large ellipse would indicate greater uncertainty.

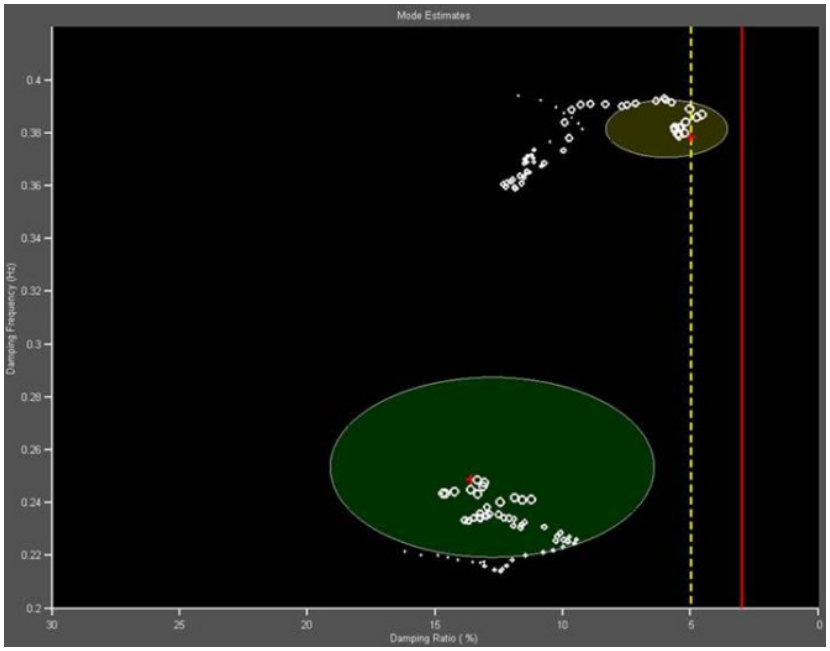

Figure 19: Improved Mode Tracking Plot with Bootstrapping Ellipse

- Capability to archive modal frequency and damping estimates for long term trending analysis thereby facilitating the ability to perform long-term correlation analysis between modal performance and other key metrics (e.g., loading on key corridors).
- Ability to rewind, playback and recreate existing Small-Signal Stability monitoring displays using historical data in memory.
- Ability to load single or multiple phasor disturbance files and perform small-signal stability type of forensics to assess the stability of the power system prior to and after the event through various analysis techniques (e.g. spectral analysis, modal analysis). For example, the tool's spectral analysis display, shown in Figure 20, lets the user to analyze the spectral content of chosen signals using three primary calculations (1) *Power Spectral Density (PSD) or Auto-Spectrum* to identify sharp peaks indicative of strong oscillatory activity observable in the signal; (2) *Coherency*: to identify a signal's correlation or participation in a particular mode; (3) *Cross Spectral Density (CSD) or Cross-Spectrum*: to identify the relative phase information associated with a particular mode (i.e. mode shape information). Note: The PSD and CSD are calculated using Welch's periodogram averaging technique – the algorithm parameter settings (e.g. time window, percent overlap, FFT window length) may be changed through a user friendly GUI.

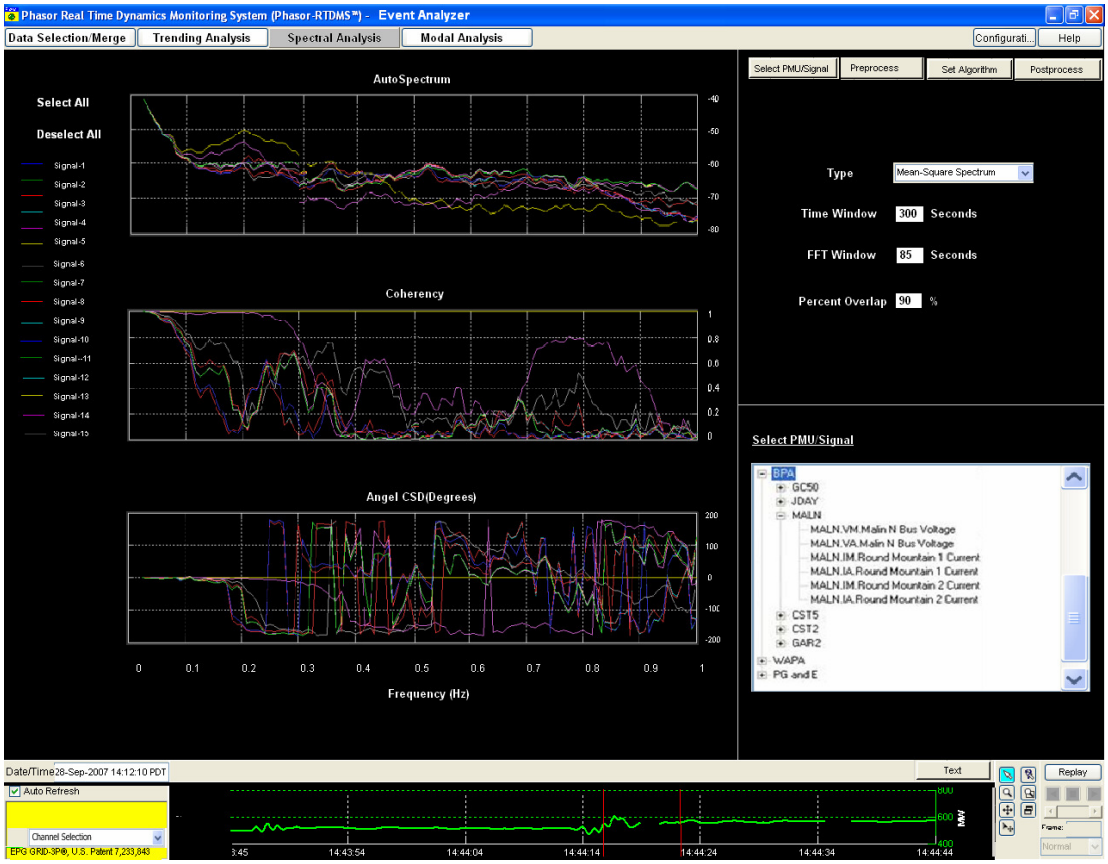

Figure 20: Sample Spectral Analysis Display.

4.0 MEASUREMENT BASED SENSITIVITIES AND VOLTAGE STABILITY MONITORING

4.1. Measurement based Sensitivities

It is well understood that with additional loading on the power system, there is degradation in the voltages across the system. This relationship is typically represented by the P-V or Q-V curves. Furthermore, the gradient at any point along such a curve provides the voltage sensitivity at that bus with respect to the loading conditions. The traditional method for obtaining this information is dependent on the system model, especially the load model, which is built by history data.

Phasor measurements offer the ability to obtain this very same information directly from the real time measurement without requiring any modeling information. In particular, PMU devices installed at a substation measure the voltage phasors (both magnitudes & angles) at a bus and the MW and MVAR flows on the monitored lines. With the precise time-synchronized alignment and the high sub-second resolution of these measurements, it is possible to trace out portions of the P-V or Q-V curves for a monitored critical load bus or corridor in real time. Additionally, there is enough loading variation within the system to estimate the local gradient of such curves which map changes in one variable (MW or MVARs) to changes in the other (voltages) – i.e., the current voltage sensitivities at that location/interface.

For illustration purposes, Figure 21 traces the P-V curves, and tracks the voltage sensitivities at the Malin 500 kV bus over time under different COI loading conditions. The sensitivities are computed using linear regression on the most recent data set collected over a 10 minute window. The results exemplify how the voltage sensitivity increases with increased loading as the system operating point moves further down along the P-V curve and closer to the voltage collapse point and can be used to anticipate low voltage problems. Additionally, is also possible to quickly detect discrete changes in the system such as control actions (e.g. insertion of cap banks), which cause these curves to shift outward (or inward).

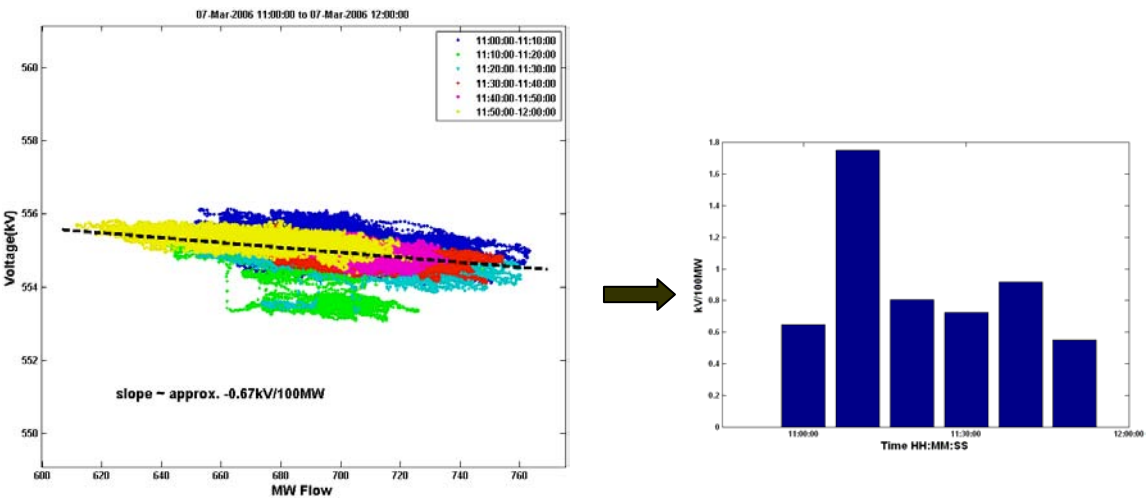

(a)

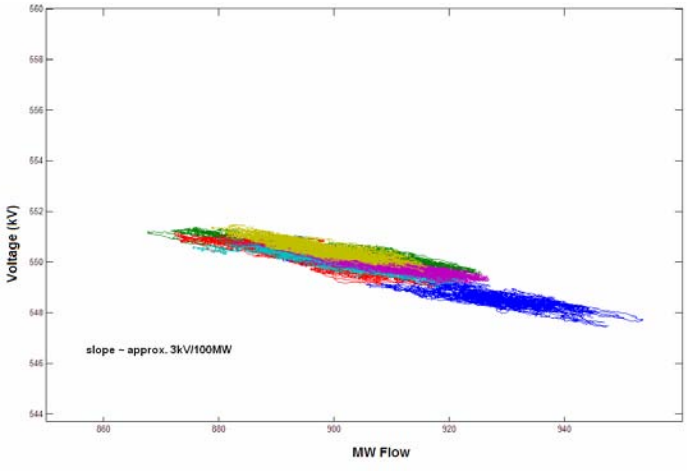

(b)

Figure 21: P-V curves and voltage sensitivities at different loading levels across COI - (a) voltage sensitivity ~ 1kV/100MW under light loading conditions (b) voltage sensitivity ~ 3kV/100MW under increased loading conditions.

Different techniques may be used to perform the regression and obtain these sensitivities: (1) least squares linear regression, and (2) orthogonal regression. Initial results suggest orthogonal regression is preferable and is less prone to inaccuracies especially when a short time window is used (Figure 22).

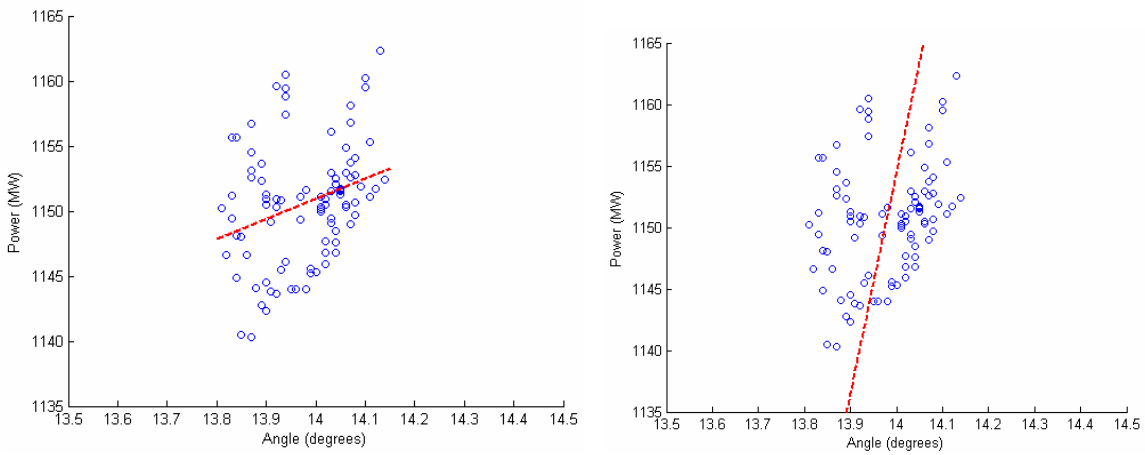

(a) (b)

Figure 22: Estimating sensitivities using (a) Least Squares Regression (b) Orthogonal Regression.

4.2. Voltage Stability Loading Margins

A literature review on the utilization phasor measurements to monitor voltage stability margins has shown that such measurements at load bus or across a key interface can also be used to estimate the maximum loading margins at the bus and define a Voltage Stability Index (VSI) for the bus/interface [8-11]. It is a well-known fact that for a two-bus system with a constant power load (i.e., a constant source behind an impedance and a load), the maximum loadability condition occurs when the voltage drop across the source impedance is equal to the voltage across the load. Hence, the idea is to use the phasor measurements at the bus to dynamically track in real-time the two-bus equivalent of the system. In particular, given the voltage and current phasor measurements at the bus ('$\overline{V}$' and '$\overline{I}$'), it is possible to estimate the parameters of the Thevenin equivalent system ('$\overline{E}_{th}$' and '$\overline{Z}_{th}$') from a sliding window of discrete samples using a recursive least squares scheme (RLS). The maximum loadability condition corresponds to the case when '$E_{th} = 2V$' and the Voltage Stability Index can be defined as:

$$VSI = \frac{V}{\Delta V} = \frac{Z_{app}}{Z_{th}} \tag{16}$$

where 'ΔV' is the voltage drop across the Thevenin equivalent impedance and 'Z_{app}' is the apparent load impedance (i.e., '$\left|\overline{V}/\overline{I}\right|$'). This indicator reaches unity at the maximum loadability point. Furthermore, since the Thevenin parameters are being tracked dynamically, they reflect any changes that may occur in the power system operating conditions and consequently provide the most accurate assessment of loadability estimates.

The very same methodology can also be used to compute Voltage Stability Index for the power transfer across a tie-line. By assuming a directional flow across the line, the line is replaced by a fictitious sink and source at the sending and receiving ends of the line respectively, that draw the same power as the tie-line flows. One can now replace the system with its Thevenin equivalent and compute the VSI for the tie-line flows as well.

Finally, if we assume that 'Z_{th}' isn't changing significantly, we can also compute a Power Margin (PM) from the two-bus equivalent as:

$$\Delta S = \left(E_{th} - Z_{th} I_{th}\right)^2 \Big/ 4Z_{th} \tag{17}$$

Again, operators may be alarmed if these indices fall below predetermined thresholds (e.g. 5% of the current load/flow).

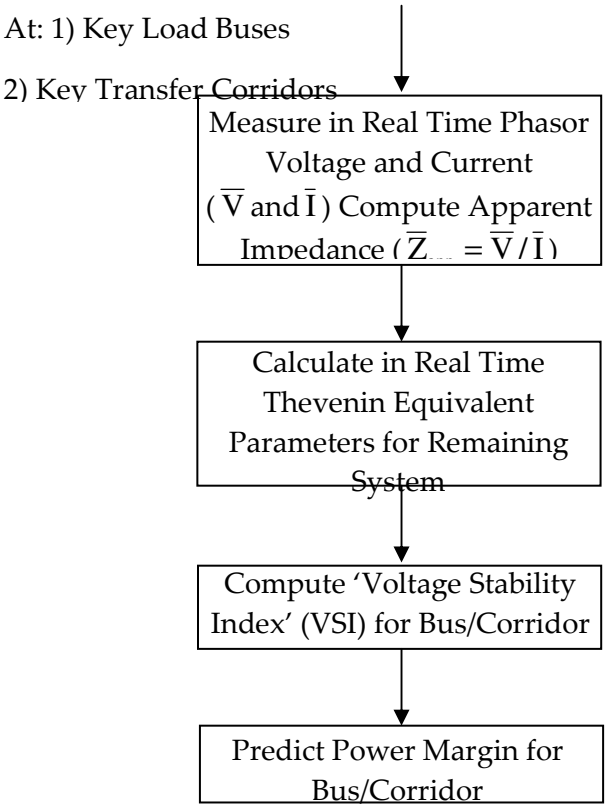

Figure 23: Flow Chart for voltage stability assessment based on phasor measurements.

More recently, a new voltage stability analysis model has been proposed for a multiple-infeed load center where both sides of the interconnection to the load are assumed to be able to provide voltage support [21]. In this model, Thevenin equivalents are estimated at both sides of

the bus (Figure 24). In order to represent correctly the loads, the equivalent resistances cannot be ignored anymore.

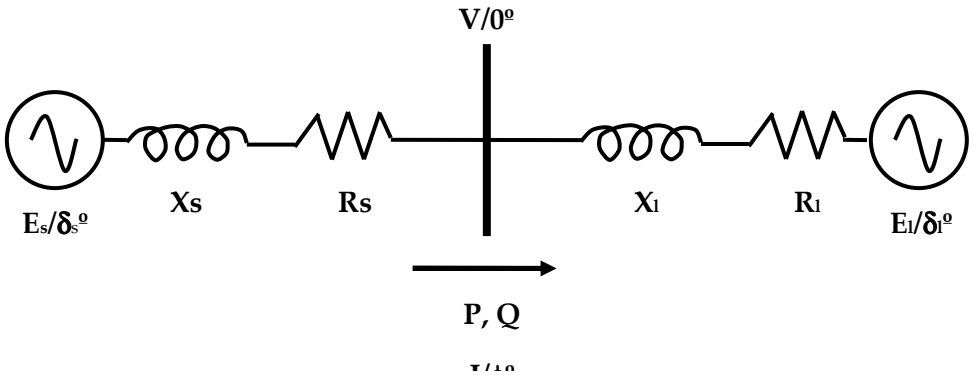

Figure 24: Voltage stability analysis model for a multiple-infeed load center using phasor measurements.

To compute the equivalent parameters of the new model, the following least squares optimization problem needs to be solved (at least three measurements are required). Besides, the accuracy of the estimation highly depends on the sampling rate: it must be chosen so that data points are not too close to each other.

$$\min_{E_s,\delta_{s_i},X_s,R_s,E_r,\delta_{r_i},X_r,R_r} \left\| \begin{matrix} E_r \sin(\delta_{r_i}) + R_r I \sin(\phi_i) + X_r I \cos(\phi_i) - V_i \\ E_S \sin(\delta_{s_i}) + R_r I \sin(\phi_i) + X_r I \cos(\phi_i) \\ E_r \sin(\delta_{r_i}) + R_r I \sin(\phi_i) + X_r I \cos(\phi_i) - V_i \\ E_r \sin(\delta_{r_i}) + R_r I_i \sin(\phi_i) + X_r I \cos(\phi_i) \\ ..... \\ ..... \end{matrix} \right\| \quad (18)$$

where: $I\cos(\phi_i) = P_i / V_i$, $I\sin(\phi_i) = -Q_i / V_i$

The first advantage of such a model is that it provides a better representation of the real power system. Indeed, the fact that voltage support may come from both sides of the bus is now taken into account. The second important feature of this model is that it estimates the voltage stability margin of the system without having to make some hypothesis on the load model. Overall, it is

its simplicity that makes this model very easy to use for real time stability estimation of a transmission path.

In order to see whether this model gives accurate results, the multiple-infeed model is tested at load center within the CA ISO. The following table presents the values of the computed equivalent Thevenin parameters:

E_s	R_s	X_s	E_l	R_l	X_l
1.066	0.067	0.034	0.989	0.01	0.041

From these results, the P-V curves can be plotted (Figure 25). This method seems to give a good estimation of the voltage stability margin. However, it should be pointed out that the model was tested in an unstressed situation. Additional studies under stressed conditions are needed to further validate the approach.

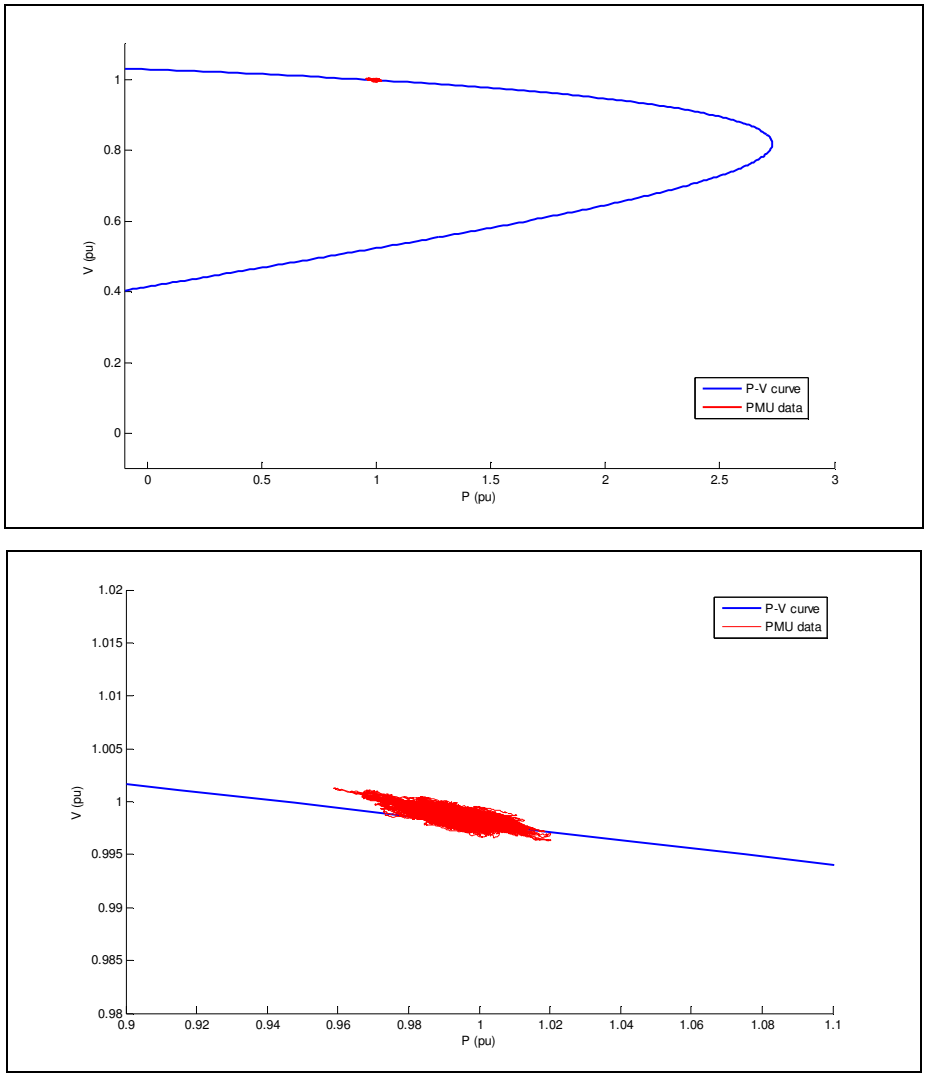

Figure 25: Estimating voltage stability margins with phasor measurements: (a) P-V curve predicted by the multiple-feed load center model; (b) phase measurement data used in the model parameter estimation.

A limitation of the above approaches is that the initial margin estimates and stability indices incur abrupt jumps when discrete events such as generator limits are reached. However, given that system voltage collapse typically occurs at slower timescales, if these algorithms are used in a real-time environment where the estimates are updating periodically at frequent intervals, then such an application should be able to provide adequate early warning to the operator in spite of the above mentioned limitation.

4.3. Predicting Voltage Stability with Phasor Measurements

The synchronized voltage measurements also serve as a time series that can be used to develop an adaptive Auto-Regressive (AR) predictive model to project the voltage trends a short interval into the future [12] (Note: A similar AR model was proposed for the small-signal stability monitoring algorithms). This approach is especially useful to ascertain the outcome of a sudden disturbance injected into the system due to a fault or an outage. An AR model is ideal for expressing a signal as a mixture of exponentially decreasing and damped sinusoidal components (i.e., ' $Ae^{\alpha t}\sin(\omega t+\beta)$ ' where 'A', 'α', 'ω' and 'β' are the strength, damping, frequency and phase respectively). Hence, given 'N' measurement samples over a predefined time window, the objective is to fit them to a 'p' order Auto-Regressive model (AR-p) given by:

$$X_t = \sum_{i=1}^{p} \phi_i X_{t-i} + a_t \tag{19}$$

where 'X_t' are the measurements, 'ϕ_i' are the model parameters (also called prediction coefficients) and 'a_t' is the white noise in the measurements. The Voltage Stability Index mentioned above can then be applied to the predicted trace for a fast stability assessment soon after the transient has been launched.

4.4. Implementation of Measurement bases Sensitivity Prototype Tool

In late 2007, the phasor visualization tool was augmented with two new displays for measurement based Angle Sensitivity and Voltage Sensitivity. This has facilitate better understanding of Voltage-(Real/Reactive) Power and Phase Angle-Real Power relationships for key corridors and at critical generation and load buses where PMUs have been installed. The associated sensitivities (in kV/100MVAR or º/100MW) are also important stability indicators with respect to voltage and transient stability, and provide real time visual alarming to operators when these sensitivities exceed acceptable thresholds.

Figure 26 is a sample operator display for monitoring measurement based sensitivities. Here, the two signal pairs (e.g., voltage at a bus and loading at bus/flows across a corridor) for which the sensitivity is to be monitored and tracked are encircled by an ellipse, which is colored as per the sensitivity alarming threshold limits. Hence, multiple groups within the geographic display are illustrative of the various signal pairs for which the sensitivity is being computed in real time. For the one selected pair (highlighted in the display), the smaller panel on the top right provides the sensitivity trends color-coded to represent normal, alert or alarm levels. The corresponding P-V curve(s) is also shown in the bottom right with the most recent data points shown in red. In Figure 26, notice how the curve moves outward over time due to changing system conditions. The ability to track these curves and sensitivities in real time purely from system measurements, and therefore presenting the actual situation, is valuable information for the operator.

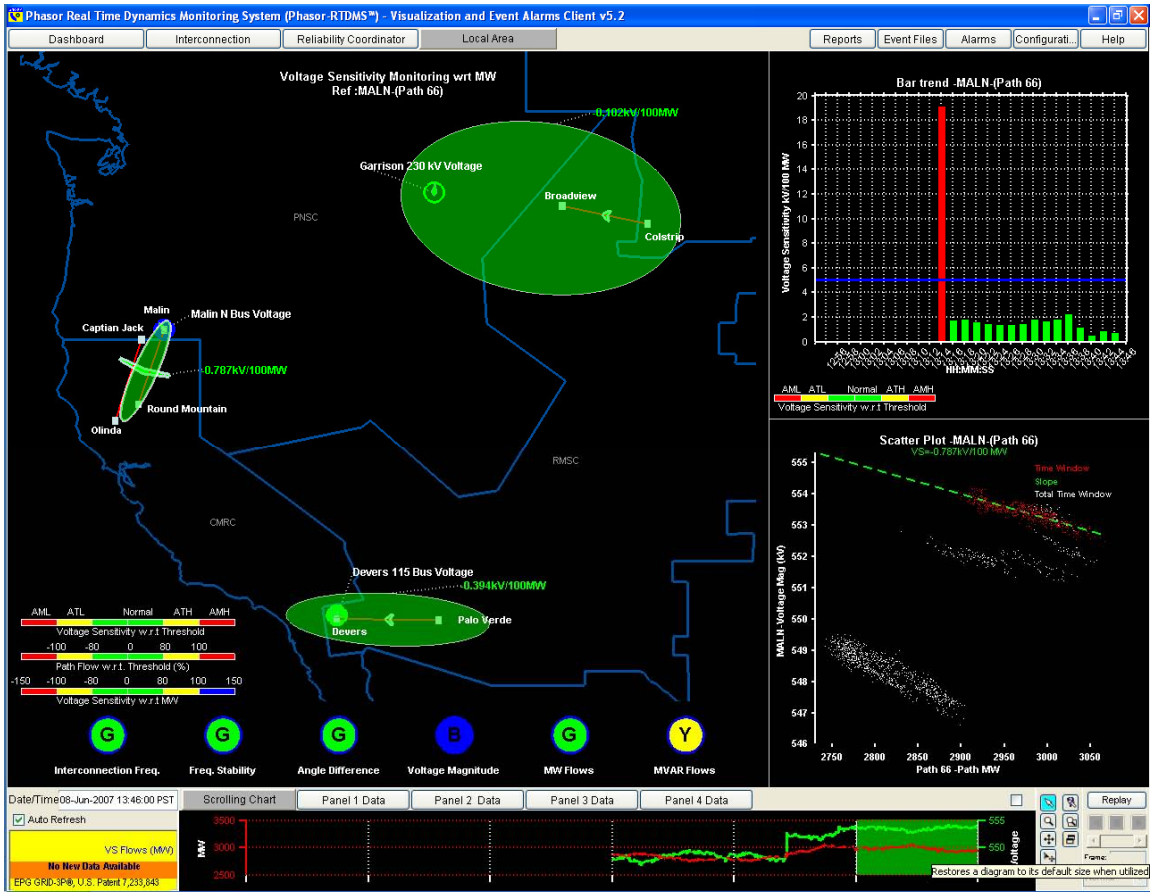

Figure 26: Voltage Sensitivity Monitoring Display

5.0 FREQUENCY RESPONSE MONITORING

A control area's contribution to frequency support is measured by the natural frequency response of its generators and load to frequency variations. It characterizes the typical frequency excursion (within the seconds timeframe) following a loss of a large generator on an Interconnection which is associated with primary control and is comprised of the following two components [13]:

- Natural arrest in frequency decline due to "load rejection" or reduced power consumption of frequency dependent loads (e.g. motors).
- The governing action of generating units responding to the declining frequency in the 3-10 seconds timeframe in an attempt to partially recover the frequency before secondary frequency regulation or Automatic Generation Control (AGC) units bring the frequency back to 60Hz or pre-event levels within 2-10 minutes (i.e., AGC time constants).

Traditionally, the frequency response characteristic ('β'), expressed in MW/0.1Hz and a measure of frequency control stiffness, is calculated using 1-minute CPS data (one-minute averages of ACE and "frequency deviation from scheduled") using the following equation [16]:

$$\text{Freq. Response}_{\text{interconnection}} = \text{Bias}_{\text{interconnection}} - (\Delta ACE_{net}/\Delta freq) \quad (20)$$

where

$\text{Bias}_{\text{interconnection}}$ = the interconnection frequency bias

ACE_{net} = the aggregate of the ACE for all the control areas in the interconnection

ΔACE_{net} = the net ACE change between two consecutive minutes

$\Delta freq$ = the frequency change between tow consecutive minutes

A larger value for 'β', expressed in MW/0.1Hz, indicates a stiffer frequency control allowing less drop following the loss of generation [14].

Although the above mentioned approach has shown merit [16], time skews between the different measurements can introduce inaccuracies and spurious results. Furthermore, given that the timescales associated with frequency response and primary control are in seconds, utilizing 1-minute data for such analysis will have its obvious limitation. The time synchronization and the higher sub-second resolution of phasor measurements overcome these restrictions and are more apt in observing frequency response following generator trips and deducing frequency response characteristics.

As an example, Figure 27 shows the frequency response captured by the WECC phasor network. These observations are consistent with following excerpt from the CA ISO event log:

"01/15/2006 - 00:24 System frequency deviated from 59.995Hz to 59.947Hz and recovered to 59.961Hz by governor action when NWE Colstrip Unit 1 relayed while carrying 240 MW. System frequency returned to pre-disturbance level at 00:29."

A straightforward calculation on this dataset shows the frequency response coefficient to be:

$$\beta = \Delta P/\Delta f = 240/(59.991\text{-}59.961) = 800\text{MW}/0.1\text{Hz} \quad (21)$$

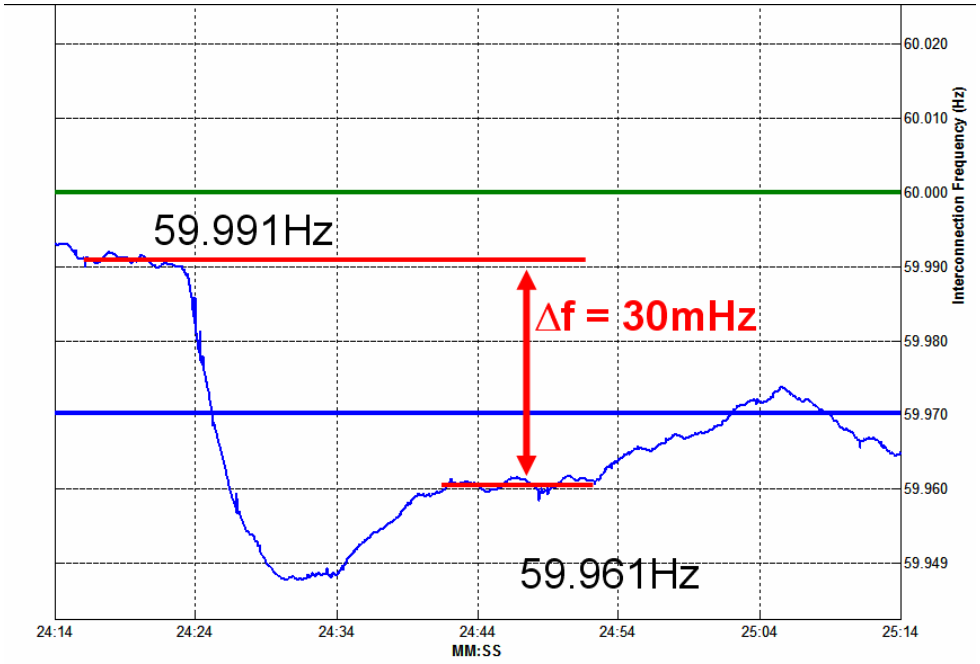

(a)

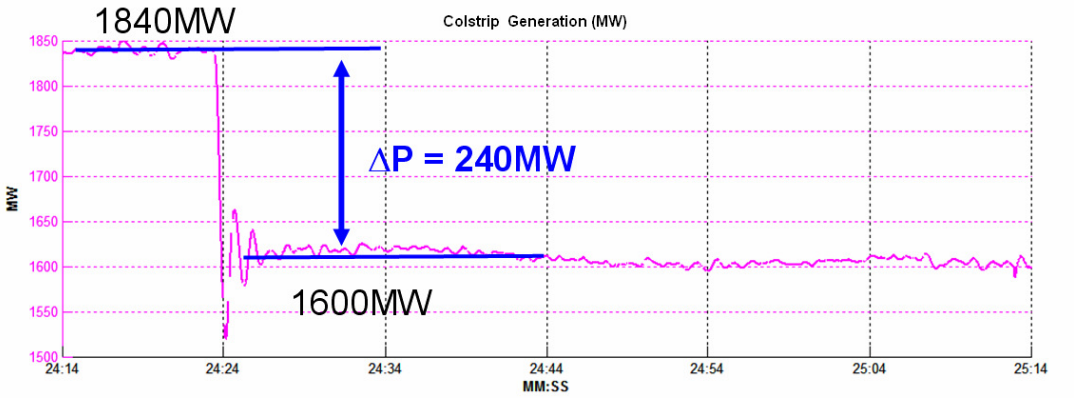

(b)

Figure 27: Frequency response captured by the phasor measurement network due to the Colstrip unit outage – (a) the interconnection frequency response to the outage (b) the ringdown observed in the MW flows from the Colstrip bus.

Previous data has shown that the frequency response can vary significantly from one generation outage to another. With frequency response characteristic being an important element for reliable grid operations, developing a historical database of such events and correlating 'β' by peak/offpeak conditions, time of day, weekday/weekend, etc towards building

a better understanding of such trends is a worthwhile effort. Furthermore this process can be automated within the phasor system application:

- Identify generator trip events using a rate-of-change trigger (a 20mHz/second rate-of-change within a 1-second window that is persistent for 2 or more seconds is proven to work well for this purpose).
- Approximate the interconnection frequency as a spatial average of geographically dispersed group of reliable PMU measurements that have been predefined.
- Calculate the relative frequency change (Δf) between the pre-event interconnection frequency and its value 10-20 seconds into the event – i.e. the timeframe associated with primary control to partially recover and stabilize the frequency.
- Inspect real powerflows out of all monitored generation stations to identify MW loss (ΔP) associated with the outage – (Note: in the case that the generation station is not monitored, this may have to be manually entered after the fact through a user interface).
- Calculate and record the frequency response characteristic ($\Delta P/\Delta f$).

6.0 GRAPH THEORY BASED PATTERN RECOGNITION

Graph theory techniques can be used to characterize, monitor and assess the global behavior of the power grid. Specifically, the correlation between any two voltage angles is a measure of the electrical connectivity amongst those points: a higher correlation coefficient implies that those two points are directly (or indirectly) electrically connected having lower net intermediate impedance between then than if the correction coefficient were of a higher value.

If, at each instance in time, one were to create a graph G={V,E}, whose nodes {V} correspond to each PMU in the system and whose edges {E} between nodes denote correlation in phasor measurements. For example, the edge e_{ij} between nodes V_i and V_j is given by $E(x_i(t)\, x_j(t))$ where $x_i(t)$ is the phasor time series at node V_j, and E() denotes expectation. Assuming an ergodic process during a measurement time window T and letting the vector X_i be denoted by $X_i = [x_i(1), ..., x_i(T)]$, we get:

$$e_{ij} = X_i^T X_i, \qquad (22)$$

Once graph G(t) is formed by this process at time t, one could then perform network level processing on this graph to elicit some user-specified information. For example, the first step could be to segment this graph into a number of strongly connected segments, each of which is weakly connected to other segments. Several methods are available for doing this; one of which is to adapt a powerful set of techniques known as spectral clustering. These methods require the evaluation of a few smallest eigenvalues and eigenvectors of the adjacency matrix A(t) of graph G(t) (Note: $A(t)_{ij} = e_{ij}$). For a power network with thousands of nodes, this method will be computationally efficient enough for real time computation.

Segmenting the graph into spectral components should prove to be a valuable way of determining the main modes of the entire network without having to monitor individual PMUs . Within each segment one could compute the average signal or the typical signal (eithera mean, median or an actual signal from a node in that segment) and this information would represent the generic steady-state or dynamic behavior for that segment.

The goal of this process is to obtain a small set of signals, one from each segment, which are sufficient to be monitored by a human operator for the purpose of real time systems monitoring. In contrast to some existing methods for obtaining a small number of monitorable signals (e.g. Principal Component Analysis), this proposed method relies on graph-theoretic analysis which considers the entire power network and its topology at each time point. The segments obtained by this method will be indicative of the extant network architecture at that time instant. Therefore the monitorable signals using this method is liable to be sensitive not only to absolute or relative signal change at each individual PMU in isolation, but also sensitive to the nature of their interaction with each other.

This method is a more efficient way of summarizing the entire phasor dataset, because it relies on a small number of strongly connected components within the network. During the summarizing process, one can ensure that no relevant data signal goes unreported. This contrasts with the PCA based methods, which monitor a pre-fixed small number of principal components and are insensitive to anomalous data, which appear merely as outliers to be rejected.

The network-level analysis approach can further be developed to perform anomaly detection at the topological level, where the entire network might be undergoing significant but incremental changes in response to an anomalous event as well as to identify the focal root cause of the anomalous behavior by evaluating graph-theoretic distance measures and other graph-theoretic tools. In particular, from the correlation of time-series data over several nodes, it is also possible to create a causality network, which is similar to the network describe earlier, but has directed edges with direction denoting causality. This kind of work has been successfully pioneered in the field of functional medical imaging. From such a causal network, the identification of the root cause or location becomes simply to look for the most highly connected node with outwardly-directed edges. As a bonus, the causal network allows for even more advanced diagnostics: one can detect not only the root cause, but also see the pattern of propagation of the anomaly across the network. It might be possible to identify risky nodes in the network after each event, and recommend corrective measures.

7.0 RTDMS SYSTEM ARCHITECTURE

The RTDMS platform for conducting phasor research and applications prototyping adheres to a Client/Server architecture where the RTDMS Data Management Server distributes the information to the RTDMS Client monitoring applications at multiple locations over LAN connection. The overall RTDMS system architecture is shown in Figure 28, and each of its different components are briefly described below.

At the CAISO, the Phasor Data Concentrator (PDC) receives multiple PDC data streams from each of the utility PDCs, packages those data streams together, and broadcasts the assembled data packet as a UDP stream in PDC Stream format. The *PDCStream/C37.118 Data Interface* has been designed to connect directly with the PDC output over a LAN, and to read in real-time the complete phasor data stream, and calculate various scaled and derived values (such as MW and MVAR). The *Data Quality Filter* component provides the capability to remove erroneous data and perform noise filtering to improve data quality. Any configuration changes, such as setting filtering options, entering PMU/Signal longitudes and latitudes, defining alarming and event archiving attributes, etc, are performed through RTDMS Data Management Server GUI.

The parsed phasor data received from the CAISO PDC and derived quantities are stored into a *Real-Time Buffer* in memory. This real-time data cache is intended to provide high performance data write/read capability for further processing or visualization. Additionally, the data will also be stored in a *SQL Database* for long-term trending and reporting purposes.

The *Alarm/Event Processor* component is designed as a Windows Service that retrieves data from the Real-Time Cache and processes this information using the set of alarming criteria. The results of the Alarm Processor and Trig Logic are saved back into the *Real-Time Buffer* for real-time alarming within the RTDMS Client applications, the SQL Server for offline alarm report generation, as well as logged into a text file for easy access within the Server. Alarming and event detection parameters are centrally configured at the RTDMS Server through the Server GUI.

Like the *Alarm/Event Processor*, the *Small-Signal Stability Module* is also an independent component that interfaces with the *Real Time Buffer* for data retrieval and results save-back. The *Small-Signal Stability Module* pre-processes the data, performs the mode estimation functions, and post-processes the answers. These results are saved back into the *Real Time Buffer* for real-time monitoring and alarming within the RTDMS Client applications, as well as the *RTDMS Database* for long-term trending. A Mode Definition GUI shall be provided on the server to centrally configure the modal estimation parameters and attributes.

The *RTDMS Client* applications (i.e. Visualization and Event Alarms, Small-Signal Stability Monitoring, Event Analyzer, etc) are stand-alone applications that can access the RTDMS Server through DCOM over a LAN connection for data retrieval from the Real-Time Cache and, its display in real-time, process this data into meaningful information, and display it using geographic and graphic displays. The *Report Generator* capability, however, retrieves data from the long-term archive (SQL database). The RTDMS displays enable the user to monitor and

track meaningful performance metrics with respect to predefined thresholds and will be alarmed whenever these thresholds are violated.

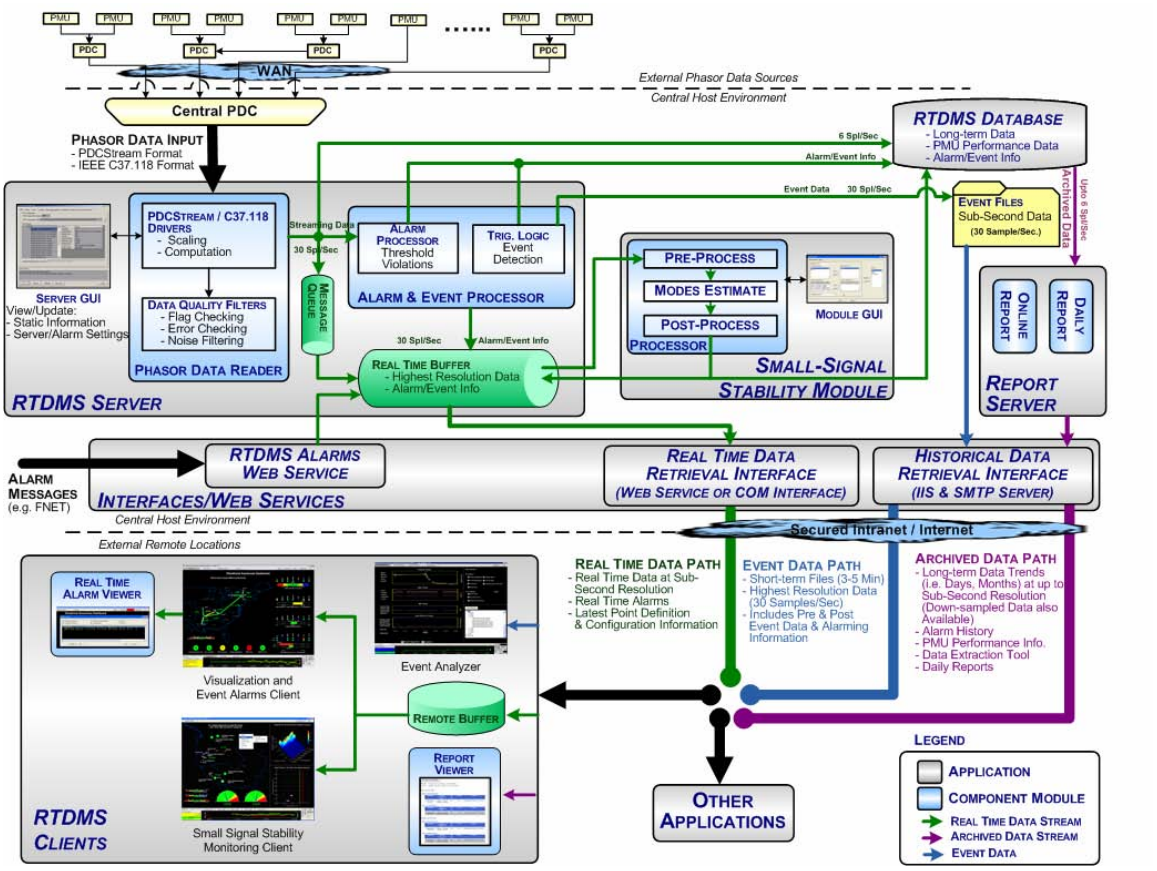

Figure 28: Real Time Dynamics Monitoring System Architecture.

8.0 CONCLUSION

This study explores various methodologies of applying phasor technology for improving stability nomograms, monitoring small-signal stability, measuring key sensitivities related to voltage stability or dynamic stability, assessing interconnection frequency response, and applying graph theory concepts for pattern recognition. Many of the ideas proposed here, such as the small-signal stability, measurement based sensitivities, etc, have already been implemented on the RTDMS phasor research platform and tested at CA ISO and BPA, while others are planned for development under a follow-on contract. The development and testing of such prototypes on the RTDMS with California ISO and BPA system operators has accelerated the adoption and use of time-synchronized phasor measurements for real-time applications in the Western Interconnection. As the network has grown and matured and RTDMS applications expanded, CA ISO has invested in upgrading the hardware infrastructure to support the system. The phasor real-time applications which initially ran on PCs/Workstation class machines in an isolated research environment have now migrated to production standards on the CAISO secure corporate network and supported by CAISO IT. The system is also operating reliably - over 90% of the devices reporting, 99% data availability, and no system down time. An indication of the improved reliability is that RTDMS is now at the Reliability Coordinator (RC) Desk in the Folsom Control Room and is an integral part of the real time operations decision making process. The system now offers a rich set of features for wide-area monitoring as well as analytics. This wide-area, common view will allow operators to evaluate stability margins across critical transmission paths, detect potential system instability in real time, and, in the future, take manual or initiate automatic actions to mitigate or dampen these potential problems. It will also enable California ISO, California and WECC utilities to explore closely related issues, such as determining the optimal location of additional phasor measurements, and to gain the experience with the technology required to develop these advanced real-time control applications.

9.0 References

1. Stoica, P., and R. Moses, *Introduction to Spectral Analysis*, Englewood Cliffs, NJ: Prentice Hall, 1997, pp. 103-106.

2. Pierre, J., D. Trudnowski, and M. Donnelly, "Initial Results in Electromechanical Mode Identification from Ambient Data," *IEEE Transactions on Power Systems*, vol. 12, no. 3, Aug. 1997, pp. 1245-1251.

3. Anderson, M., N. Zhou, J. Pierre, and R. Wies, "Bootstrap-Based Confidence Interval Estimates for Electromechanical Modes from Multiple Output Analysis of Measured Ambient Data," *IEEE Transactions on Power Systems*, vol. 20, no. 2, May 2005, pp. 943-950.

4. Van Overschee, P., B. De Moor, *Subspace Identification: Theory, Implementation, Application*, Dordrecht: Kluwer Academic publishers, 1996.

5. Ljung, L., *System Identification: Theory for the User*, 2nd Ed., Prentice Hall, 1999.

6. Zhou, N. and J. Pierre, "Electromechanical Mode Estimation of Power Systems from Injected Probing Signals Using a Subspace Method," *Proceedings of North American Power Symposium (NAPS),* August 2004.

7. D. J. Trudnowski, J. R. Smith, T. A. Short, and D. A. Pierre, "An Application of Prony Methods in PSS Design for Multimachine Systems," *IEEE Transactions on Power Systems*, vol. 6, no. 2, pp. 118-126, Feb. 1991.

8. K. Vu, M.M. Begovic, D. Novosel, M.M. Saha, "Use of Local Measurements to Estimate Voltage-Stability Margin", *IEEE Transactions on Power Systems*, Vol. 14, No. 3, Aug. 1999, pp. 1029-1035.

9. D.E. Julian, R.P. Schulz, K.T. Vu, W.H. Quaintance, N.H. Bhatt, D. Novosel, "Quantifying Proximity to Voltage Collapse Using the Voltage Instability Predictor (VIP)", 2000 IEEE Power Engineering Society Summer Meeting, Vol. 2, 16-20 Jul. 2000, pp. 931-936.

10. W.H. Quaintance, K. Uhlen, D.E. Julian, J.O. Gjerde, K.T. Vu, L.K. Vormedal, "Raising Energy Transfer in Corridors Constrained by Voltage Instability - Statnett Case", 2000 IEEE Power Engineering Society Summer Meeting, Vol. 4, 16-20 Jul. 2000, pp. 2021-2026.

11. B. Milosevic, M. Begovic, "Voltage-Stability Protection and Control Using a Wide-Area Network of Phasor Measurements", *IEEE Transactions on Power Systems*, Vol. 18, No. 1, Feb. 2003, pp. 121-127.

12. C. Xu, J. Liang, Z. Yun, L. Zhang, "The Small-Disturbance Voltage Stability Analysis through Adaptive AR Model Based on PMU," *IEEE/PES Transmission and Distribution Conference & Exhibition*, Dalian, China, 2005.

13. NERC Frequency Task Force of the NERC Resources Subcommmittee, “Frequency Response Standard Whitepaper - Draft”, October 2003.

14. R.P. Schulz, “Modeling of Governing Response in the Eastern Interconnection”, Proc. 1999 Winter Meeting IEEE Power Engineering Society, pp. 561-566.

15. J. Ingleson & M. Nagle, “Decline of Eastern Interconnection Frequency Response,” presented at 1999 Fault & Disturbance Conference, Georgia Tech, May 3-4, 1999.

16. NERC Training Resources Working Group, “NERC Training Document – Understand and Calculate Frequency Response,” February 20, 2003.

17. A. G. Phadke, "Synchronized phasor measurements in power systems", IEEE Computer Applications in Power, Vol. 6, Issue 2, pp. 10-15, April 1993.

18. J. Shi and J. Malik, “Normalized Cuts and Image Segmentation”, IEEE Transactions on Pattern Analysis and Machine Intelligence, Vol. 22, No. 8, August 2000.

19. R. Myers, R. C. Wilson, and E. R. Hancock, “Bayesian Graph Edit distance” IEEE Transactions on Pattern Analysis and Machine Intelligence, Vol. 22, No. 6, June 2000.

20. Y. Chen, G. Rangarajan, J. Feng, M. Ding, 2004 “Analyzing multiple nonlinear time series with extended Granger causality”. Physics Letters A 324, 26-35.

21. M. Parniani, J.H. Chow, L. Vanfretti, B. Bhargava, and A. Salazar, :Voltage Stability Analysis of a Multiple-Infeed Load Center Using Phasor Measurement Data, *2006* IEEE/PES Power Systems Conference and Exposition (IEEE Cat No. 06EX1305C), p 7 pp. 1299-1305, Nov. 2006.

BUS NAME	PSD (L,S, N) 0.265 Hz	Ref. = GC50 0.265 Hz Cxy, angle	PSD (L,S, N) 0.385 Hz	Ref. = GC50 0.385 Hz Cxy, angle	PSD (L,S, N) 0.400 Hz	Ref. = AULT 0.400 Hz Cxy, angle	PSD (L,S, N) 0.60 Hz	Ref. = DV01 0.60 Hz Cxy, angle	PSD (L,S, N) 0.616 Hz **Sharp peak**	Ref. = SYLM 0.616 Hz Cxy, angle
GC50.VA.Grand Coulee Hanford Voltage	L	Reference	L	Reference	N		N		N	
JDAY.VA.John Day Bus Voltage	L	1.0, 0 deg.	L	1.0, 0 deg.	N		N		N	
MALN.VA.Malin N.Bus Voltage	L	1.0, 0 deg.	L	1.0, 0 deg.	N		N		N	
COLS.VA.Colstrip Bus Voltage	L	0.95, 0 deg.	L	0.90, 0 deg.	N		N		N	
SYLM.VA.Sylmar Bus Voltage	L	0.90, 180 deg.	L	0.90, 180 deg.	N		N		L	Reference
MPLV.VA.Maple Valley Bus Voltage	L	1.0, 0 deg.	L	1.0, 0 deg.	N		N		N	
SUML.VA.Summer Lake 500 kV Voltage-N	L	1.0, 0 deg.	L	1.0, 0 deg.	N		N		N	
MCN5.VA.McNary 500 kV Voltage-S	L	1.0, 0 deg.	L	1.0, 0 deg.	N		N		N	
AULT.VA.Ault 345 kV Voltage (Craig)	N		N		L	Reference	N		N	
BEAR.VA.Bears Ears 345 kV Bus Voltage (B	N		N		L	1.0, 0 deg.	N		N	
SHIP.VA.Shiprock 345 kV Voltage (San Jua	S	0.6, 180 deg.	N		L	0.75, 0 deg.	N		L	0.1
VN01.VA.Vincent 230 kV Voltage	L	0.90, 180 deg.	L	0.90, 180 deg.	N		N		L	0.75, 0 deg.
DV01.VA.Devers 500 KV Bus Voltage	L	0.90, 180 deg.	L	0.90, 180 deg.	N		L	Reference	N	
MDW5.VA.MIDWAY Bus Voltage	L	0.95, 0 deg.	L	0.9, 0 deg.	N		L	0.75, 180 deg.	S	0.75, 180 deg.
ML50.VA.ML500 Bus Voltage	L	0.97, 0 deg.	L	0.95, 0 deg.	N		L	0.75, 180 deg.	S	0.75, 180 deg.
PTSB.VA.PITSBG Bus Voltage	L	0.97, 0 deg.	L	0.95, 0 deg.	N		L	0.75, 180 deg.	S	0.75, 180 deg.

NOTES:

1. PSD content (L = large, S = small, N = none).
2. The 0.265-Hz mode is the N-S intertie mode.
3. The 0.385-Hz mode has a similar shape as the 0.265-Hz mode. It is likey the Alberta mode; we have no measurements from Alberta to verify this.
4. The 0.616-Hz sharp peak is likely an aliasing artifact due to the DC converters.
5. The 0.60-Hz mode is likely a southern California vs. the middle of California. Much of the spectral information is "masked" by the 0.616-Hz aliasing peak.
6. The 0.65-Hz mode is likely the BC Hydro vs. the northern US.

Table 1: Spectral content of WECC data